Journal Pre-proof

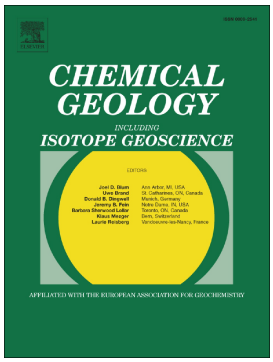

Biotite reactivity in nitric and oxalic acid at low temperature and acid pH from surface and bulk dissolution measurements

Chiara Cappelli, Jordi Cama, Alexander E.S. Van Driessche, F. Javier Huertas

PII: S0009-2541(20)30345-4

DOI: https://doi.org/10.1016/j.chemgeo.2020.119806

Reference: CHEMGE 119806

To appear in: *Chemical Geology*

Received date: 1 April 2020

Revised date: 30 July 2020

Accepted date: 31 July 2020

Please cite this article as: C. Cappelli, J. Cama, A.E.S. Van Driessche, et al., Biotite reactivity in nitric and oxalic acid at low temperature and acid pH from surface and bulk dissolution measurements, *Chemical Geology* (2020), https://doi.org/10.1016/j.chemgeo.2020.119806

Biotite reactivity in nitric and oxalic acid at low temperature and acid pH from surface and bulk dissolution measurements

Chiara CAPPELLI[1,*,#], Jordi CAMA[2], Alexander E.S. VAN DRIESSCHE[3], F. Javier HUERTAS[1]

[1] *Instituto Andaluz de Ciencias de la Tierra – IACT (CSIC-University of Granada), 18100 Armilla (Granada), Spain*

[2] *Institute of Environmental Assessment and Water Research-IDAEA (CSIC), 08034 Barcelona, Catalonia, Spain*

[3] *Université Grenoble Alpes, Université Savoie Mont Blanc, CNRS, IRD, IFSTTAR, ISTerre, F-38000, France*

* Corresponding authors

Present address: *Department of Geological Sciences, The University of Alabama, Tuscaloosa, AL 35487, USA*

ABSTRACT

The dissolution of biotite, a trioctahedral mica, was investigated for a temperature range of 25-70 ºC and a pH range of 1-3 in the presence of HNO_3 (nitric acid) and $H_2C_2O_4$ (oxalic acid) solutions. Single millimetric, cleaved flakes of biotite were reacted in batch and flow-through experiments to obtain kinetic information and elucidate the mechanisms that control the overall dissolution reaction under these conditions. The reacting basal surface was explored using in-situ laser confocal microscopy (LCM-DIM) and ex-situ scanning and phase shifting interferometry (VSI-PSI), while the release of tetrahedral (Al and Si), octahedral (Mg and Fe) and exchange (K) cations in solution was monitored over time. This experimental approach allowed us to calculate far-from-equilibrium dissolution rates associated with changes in topography of the (001) surface (horizontal retreat (R_{step}) and vertical retreat ($R_{vertical}$)), etch pit formation and growth (R_{pit}) and the release of Si in solution, i.e., bulk dissolution ($R_{bulk,Si}$). In HNO_3 solutions, a proton promoted reaction mechanism (PPRM), through proton adsorption on the biotite surface, was dominant. The variation of R_{step}, $R_{vertical}$ and $R_{bulk,Si}$ accounting for the dissolution of (hk0) surfaces at different temperature and pH was used to calculate the apparent activation energy (E_a) and the proton reaction order (n_{H+}). The respective values decreased from 63 kJ mol^{-1} at pH 1 to 31 kJ mol^{-1} at pH 3 and increased from 0.46 at 25 °C to 0.77 at 70 °C. This variability was related to the variation of proton consumption with temperature. In $H_2C_2O_4$ solutions, formation and growth of etch pits on the (001) surface occurred, yielding an increase in surface roughening. R_{pit} accounted for the rate of etch pit development which was observed to increase, as temperature increased. Based on R_{pit}, relatively high E_a values (121 kJ mol^{-1} and 162 kJ mol^{-1}) were associated with an early evolution of the basal etch pits, whereas lower values (36 kJ mol^{-1} and 56 kJ mol^{-1}) were calculated using $R_{bulk,Si}$. The present study contributes to the interpretation of the mechanisms involved in the biotite dissolution process at highly acidic pH, in the presence of inorganic and organic acid, and low temperature ($T \leq 80$ ºC). Furthermore, our results highlight the importance of combining surface and bulk analyses to assess the balance between the different reactions involving proton consumption during the dissolution and its dependency on temperature, pH and organic acids concentration.

1. INTRODUCTION

Dissolution of phyllosilicates (sheet silicates) plays a central role in a wide array of geochemical processes occurring in both natural and engineered environments, such as metal cycling, sequestration of contaminants and soil fertility (Brantley, 2008). A detailed knowledge of the dissolution reaction mechanisms related to the environmental variables (e.g. pH, temperature, organic matter, chemical affinity or ionic strength) is necessary to better understand the reactivity of phyllosilicates.

Either experimental or theoretical approaches are commonly employed to study the reactivity of phyllosilicates in aqueous solutions (e.g. Kurganskaya and Luttge, 2013). In the case of experimental studies, two approaches have been adopted to quantify the dissolution rates of phyllosilicates: bulk solid/solution chemistry analysis and in situ/ex situ observation of the basal surface-solution interface. For example, to study the dissolution kinetics of clays and micas (e.g. Cama and Ganor, 2015 and references therein), bulk rates have been calculated using powder samples placed in flow-through and batch experiments, where all mineral surfaces react with the fluid (Amram and Ganor, 2005; Bauer and Berger, 1998;; Cama et al., 2000; Cama et al., 2002; Cappelli et al., 2018; Carroll and Walther, 1990; Chin and Mills, 1991; Devidal et al., 1997; Furrer et al., 1993; Ganor et al., 1995;;; Huertas et al., 1999;; Kalinowski and Schweda, 2007; Köhler et al., 2003; Lammers et al., 2017;; Malmström et al., 1996; Murakami et al., 2003; Nagy et al., 1991; Oelkers et al., 2008; Rozalén et al., 2008; Samson et al., 2005; Smith et al., 2017; Swoboda-Colberg and Drever, 1993; Taylor et al., 2000;; Wieland and Stumm, 1992; Yang and Steefel, 2008; Zysset and Schindler, 1996). Detailed observations of dissolution and (re)-precipitation reactions taking place at basal surfaces using surface analytical microscopies (Atomic Force Microscopy (AFM), Vertical Scanning and Phase Shifting Interferometry (VSI and PSI) and laser confocal microscopy (LCM-DIM) have provided key insights into the reactivity of various clays and micas (apophyllite and phlogopite (Aldushin et al., 2004; Aldushin et al., 2006)); biotite (Cappelli et al., 2015; Cappelli et al., 2013; Haward et al., 2011; Li et al., 2014; McMaster et al., 2008); hectorite and nontronite (Bickmore et al., 2001); muscovite (Kurganskaya et al., 2012; Kurganskaya and Luttge 2013); smectite (Satoh et al., 2013; Yokoyama et al., 2005)). These advanced microscopy techniques have proved to be the basis for developing realistic simulations of mineral reactivity (e.g. Kinetic Monte Carlo (KMC) simulations (Kurganskaya and Lüttge, 2013; Lüttge et al., 2013; Luttge et al., 2019)).

Bulk dissolution rates are usually normalized to the reactive surface area, which is calculated using BET specific surface area measurements (e.g. biotite (Hodson, 2006), smectite (Metz et al., 2005; Rozalén et al., 2008)). Single surface dissolution rates, sometimes

referred to as absolute rates (Arvidson et al., 2003; Dove and Platt, 1996; Fischer et al., 2012), have been obtained from the temporal variation in the reactive surface topography (e.g., phlogopite (Aldushin et al., 2006), chlorite (Brandt et al., 2003), biotite and muscovite (Kuwahara, 2008; Pachana et al., 2012), smectite (Satoh et al., 2013; Yokoyama et al., 2005)). The resulting dissolution rates obtained from both approaches yield rate versus pH and rate versus temperature dependencies that compare poorly, hindering our interpretation of the reaction kinetics and surface reactivity of phyllosilicates.

The dissolution of micas, an important group of phyllosilicates, has been extensively investigated using both bulk chemistry analysis and surface observation (e.g., Acker and Bricker, 1992; Aldushin et al., 2007; Aldushin et al., 2006; Bray et al., 2014; Bray et al., 2015; Haward et al., 2011; Kalinowski and Schweda 1996; Kurganskaya and Luttge 2013; Lamarca-Irisarri et al., 2019; Rufe and Hochella, 1999). In this study, we attempt to further improve the understanding of micas reactivity through the quantification of the dissolution rates of biotite (trioctahedral mica) under identical conditions using both bulk and single surface approaches. Cleaved biotite flakes were reacted in batch and flow-through reactors under a temperature range of 11.5-80 °C and a pH range of 1-3 using inorganic nitric (HNO_3) and organic oxalic ($H_2C_2O_4$) acids. The temporal variation in the aqueous chemistry was used to extract bulk dissolution rates while variations in surface dynamics and topography of the (001) surface were measured in situ by LCM-DIM and ex situ by VSI and PSI, respectively. These techniques were used to determine dissolution rates for defined surface regions. The combination of both experimental approaches enabled us to obtain rate dependencies on pH and temperature in the presence of nitric and oxalic acid.

For the interpretation of the pH and T dependencies of the dissolution rates, we considered previous kinetic-related studies for biotite dissolution in acid pH using inorganic acids (Acker and Bricker, 1992; Turpault and Trotignon, 1994; Kalinowski and Schweda, 1996; Malmström and Banwart, 1997; Pachana et al., 2012; Cappelli et al., 2013) and organic acids (McMaster et al., 2008; Balland et al., 2010; Haward et al., 2011; Li et al, 2014; Voinot et al., 2013; Bray et al., 2015; Zhang and Jun, 2015). Under acidic and ligand-free conditions, these prior studies demonstrated that the biotite dissolution rate increases with decreasing pH and increasing temperature. The values for the proton reaction order (n_{H^+}) (Acker and Bricker, 1992; Turpault and Trotignon, 1994; Kalinowski and Schweda, 1996; Malmström and Banwart, 1997) and apparent activation energy (E_a) (Cappelli et al., 2013) have been used in proposed dissolution rate laws (Lasaga, 1998), defined as:

$$Rate_{H^+} = k_{H^+} \cdot a_{H^+}^{n_{H^+}} \cdot e^{\frac{-E_a}{RT}} \cdot f(\Delta G_r) \qquad (1)$$

where k_{H+} refers to a rate constant under acidic conditions, a_{H+} is the proton activity, R and T are the gas constant and absolute temperature, and the $f(\Delta G_r)$ term accounts for the reaction deviation from equilibrium. In the case of organic ligands (e.g. citric and oxalic acids), a number of studies have shown that dissolution rates of clays and micas under acidic conditions are faster than in ligand-free solutions (kaolinite: Cama and Ganor, 2006; smectite: Golubev et al., 2006; biotite: Balland et al., 2010; McMaster et al., 2008; Haward et al., 2011; Li et al., 2013; montmorillonite: Ramos et al., 2014). In addition, it has been concluded that the overall dissolution rate is the sum of the rates of two independent mechanisms (Furrer and Stumm, 1986): a proton promoted reaction mechanism (PPRM), in which proton adsorption on the mineral surface enhances the dissolution of the mineral; and a ligand (oxalic) promoted reaction mechanism (L(O)PRM) in which an oxalate is adsorbed on the mineral surface, weakening the bonds, and as a result the mineral dissolution rate is enhanced (Cama and Ganor, 2006; Golubev et al., 2006; Ganor et al., 2009 and references therein; Ramos et al., 2011; Ramos et al., 2014). Therefore, considering the above, in acidic oxalate solutions and for far-from-equilibrium conditions (i.e. $f(\Delta G_r) = 1$), the overall dissolution rate is expressed as the sum of the PPRM rate and the OPRM rate, as:

$$Rate_{overall} = R_{PPRM} + R_{OPRM} = k_{H+} \cdot a_{H^+}^{n_{H^+}} \cdot e^{\frac{-E_{a;H+}}{RT}} + k_{ox} \cdot a_{ox}^{n_{ox}} \cdot e^{\frac{-E_{a;ox}}{RT}} \qquad (2)$$

where k_{ox} is the rate constant in the presence of oxalic acid, a_{ox} is the oxalic activity, and $E_{a;H+}$ and $E_{a;ox}$ are the apparent activation energies associated with PPRM and OPRM, respectively.

The main goal of this study was to elucidate the role that PPRM and OPRM play in the biotite dissolution under highly acidic conditions in the presence of nitric and oxalic acid. Using biotite flakes instead of powder samples in the experiments allowed us to identify the mechanisms responsible for the surface reactions. In the presence of nitric acid, both pH and temperature effects on biotite dissolution rate were studied considering that the surface-proton interaction drives the overall reaction. In the presence of the organic acid, we also considered a possible catalytic effect of the ligand on the inorganic rate and possible oxalate mechanisms intervening in the overall reaction (Eq. (2)).

2. MATERIALS AND METHODS

2.1 Sample characterization

Biotite from the Bancroft region (Ontario, Canada), purchased from Ward's Natural Science Establishment, was used in the present work. Its chemical composition was determined by a CM20 Philips transmission electron microscope (TEM) operated at 200 kV and equipped with a device for analytical electron microscopy (AEM; EDAX©). The AEM

spectra were collected in STEM mode on areas of 200 and 1000 Å, using a 70 Å diameter spot, for 15 and 50 s in order to check volatilization of light elements. Under these conditions, AEM results are considered to be quantitatively reliable (Hughes et al., 1990; Peacor, 1992). Assuming that all iron was present as Fe^{2+}, the structural formula was calculated to be

$$K_{0.97}(Mg_{1.40}Fe_{1.29}Al_{0.04}Ti_{0.09}Mn_{0.09})(Al_{0.97}Si_{3.03})O_{10}(OH)_2$$

This stoichiometry is consistent to that reported by Turpault and Trotignon (1994) and Samson et al. (2005) who used similar biotite samples.

Large flakes with a cleaved (001) surface of approximately 100 mm^2 and 0.08-0.15 mm thick were placed in batch experiments for ex situ VSI/PSI measurements. Smaller flakes with cleavage (001) surfaces of approximately 16 mm^2 and 0.08-0.15 mm thick were used in the flow-through experiments. The BET specific surface area of these small flakes was measured using 5-point N_2 adsorption isotherms with a Micromeritics ASAP 2000 surface area analyzer, degassing the sample with nitrogen for 2 h at 137 °C. The specific surface area was 0.42 ± 0.04 m^2 g^{-1}.

2.2 Experimental setup

2.2.1 Batch experiments

Batch reactors immersed in a thermostatic water-bath held at constant temperature or placed in a pre-heated oven were used to dissolve biotite in the presence of nitric acid and oxalic acid over a temperature range of 25 to 80 °C (Table 1). Single large flakes were placed in high density polyethylene bottles filled with 250 mL of 0.1, 0.01 and 0.001 mol L^{-1} HNO_3 (pH = 1, 2 and 3, respectively) or 0.1 and 0.01 mol L^{-1} oxalic acid solutions (pH = 1.4 and 2.2, respectively) and 0.01 mol L^{-1} $NaNO_3$ as the background electrolyte to reach ionic strength of ≈ 0.01 M at pH 2 and 3. Acidic conditions facilitate microscopy observation of surface dissolution features. To ensure and maintain that the solutions were undersaturated with respect to biotite during HNO_3 experiments, the input solutions of lengthy experiments (i.e. experimental run > 100 h (pH 1), > 300 h (pH 2) and > 500 h (pH 3)) were renewed at regular time intervals (Table 1).

Table 1. Experimental conditions for the batch experiments (VSI/PSI measurements).

pH	Experiment	T (°C)	Initial mass (g)	Duration (h)	solution changes	HNO_3	$H_2C_2O_4$ (M)
1	B1	25	0.08	1194	6	0.1	
	B2	40	0.05	504	2	0.1	
	B3	50	0.05	183	1	0.1	
	B4	70	0.03	284	1	0.1	
	B5	80	-	96	-	0.1	
2	B6	25	0.06	2087	11	0.01	
	B7	40	0.07	670	3	0.01	
	B8	40	0.03	1026	5	0.01	

	B9	50	0.03	560	3	0.01	
	B10	50	0.08	496	2	0.01	
	B11	70	0.04	458	2	0.01	
	B12	70	0.03	335	-	0.01	
3	B13	25	0.03	2693	7	0.001	
	B14	40	0.02	577	2	0.001	
	B15	70	0.07	192	-	0.001	
1.3	B1ox	25	0.08	212	-		0.1
	B2ox	40	0.07	72	-		0.1
	B3ox	40	0.07	191	-		0.1
	B4ox	50	0.04	72	-		0.1
	B5ox	50	0.05	191	-		0.1
	B6ox	70	0.05	192	-		0.1
2.1	B7ox	25	0.02	212	-		0.01
	B8ox	40	0.02	191	-		0.01
	B9ox	50	0.07	72	-		0.01
	B10ox	50	0.04	191	-		0.01
	B11ox	70	0.04	192	-		0.01
	B12ox	70	0.05	72	-		0.01

Selected areas (~1 mm^2) of the pristine biotite basal (001) surface were covered with a high-temperature silicone rubber (Pertex HI-T RTV). These spots were preserved from dissolution and used as reference surfaces for the VSI/PSI measurements. After the completion of each experiment, the flakes were retrieved, gently washed with abundant Milli-Q (Nanopure) water, dried, and the rubber masks were carefully removed. The differences in height between unreacted and reacted (001) surfaces were determined using either a Zemapper vertical scanning interferometer (Zemetrics) equipped with a 2048 × 2048 pixel CCD camera and 10× and 100× Mirau objectives or a phase shifting interferometer (PSI) equipped with a Linnik objective (Sensofar). The vertical and lateral resolutions of the system are better than 2 nm and 1.2 µm, respectively.

2.2.2 Flow-through experiments

Single small biotite flakes (exposed surface ≈ 16 mm^2) were placed in a custom-designed flow-through observation cell mounted on a LCM-DIM setup (a confocal system (FV300, Olympus) attached to an inverted optical microscope (IX70, Olympus)) to measure in situ the step retreat on the (001) cleavage surface. Details of this technique (e.g., vertical and horizontal resolutions) and the experimental setup can be found in Van Driessche and Sleutel (2013) and Cappelli et al. (2013). The flakes were reacted with 0.1 mol L^{-1} HNO_3 (pH ≈ 1) and 0.01 mol L^{-1} $NaNO_3$ solutions (Table 2). The experiments lasted from 2 hours up to 6 days as a function of the experimental conditions (e.g., the lower the temperature, the longer the experimental run). Images of the (001) cleavage surface were taken every 20 s to 15 min with a capture time of 9.6 s. Repetitions were performed for each experiment.

Table 2. Experimental conditions for the flow-through experiments (LCM-DIM measurements) performed at pH 1.

Experiment	T (°C)	flow rate (mL min^{-1})	HNO_3 (M)	$NaNO_3$ (M)	duration (h)
B11.5-1	11.5	0.072	0.10	0.01	142
B11.5-1b	11.5	0.072	0.10	0.01	90
B25-1	25.0	0.072	0.10	0.01	31
B25-2	25.0	0.072	0.10	0.01	18
B40-1	40.0	0.073	0.10	0.01	4
B40-2	40.0	0.073	0.10	0.01	4
B50-1	50.0	0.010	0.10	0.01	98
B50-2	50.0	0.010	0.10	0.01	25
B70-1	70.0	0.068	0.10	0.01	5
B70-2	70.0	0.068	0.10	0.01	2
B70-3	70.0	0.072	0.10	0.01	2

2.3. Solutions and analysis

All input solutions were prepared using analytical reagent grade HNO_3, oxalic acid, $NaNO_3$ (Sigma-Aldrich) and Milli-Q (Nanopure). The pH of the input and output solutions was measured with a combined glass electrode (CrisonTM) at room temperature (22 ± 2 ºC), yielding pH values with an accuracy better than 0.02 pH units; pH calibration was done with standard pH 2, pH 4 and pH 7 buffer solutions. Total concentrations of Si, Al, Mg, K and Fe were measured in the output solutions of the batch experiments. Silica concentrations were determined by colorimetry, using the molybdate (molybdenum) blue method (Grasshoff et al., 2009) with a Visible/UV spectrophotometer. The maximum of absorption was measured at 825 nm using a UV/Visible Perkin Elmer Lambda 25 spectrometer. The detection limit was 5 ppb and the uncertainty was smaller than 3%. The aluminum concentrations were measured by spectrofluorimetry using lumogallion as a complexing agent (Howard et al., 1986). A FluoDia T70 High Temperature Fluorescence Microplate Reader was used with excitation and emission wavelengths of 486 and 550 nm, respectively. The detection limit was 2 ppb and the uncertainty was smaller than 5%. The concentrations of Mg and K were determined by ion chromatography using a Methrohm 883 Basic IC plus with a Metrosep C3 column. The detection limit and the uncertainty for Mg and K concentration analyses were 0.5 ppb and 3%, respectively. The Fe concentration was determined by colorimetry, measuring the absorption of the Fe (II)-1,10–phenanthroline complex (Lazic et al., 2010; Pyenson and Tracy, 1945). The detection limit was 0.2 ppm and the uncertainty was less than 3%.

In the presence of oxalic acid, colorimetry could not be used to measure Si and Al concentrations owing to the interference with organic species. Thus, total Si and Al concentrations were analyzed by inductive coupled plasma-atomic emission spectrometry (ICP-AES; Thermo Jarrel-Ash with CID detector and a Perkin Elmer Optima 3200 RL). The detection limits for Si and Al were 13 and 40 ppb, respectively. The accuracy of the measurement was estimated to be 3%.

2.4 Calculation of dissolution rates

Batch experiments were used to measure dissolution rates associated with basal surface dissolution. In nitric acid solutions, a vertical dissolution rate ($R_{,vertical}$) was obtained using ex situ VSI and PSI measurements and using the preserved unreacted surfaces as reference surfaces. The change in surface height was determined between a reacted and an unreacted surface of a selected surface region. Thus, $R_{,vertical}$ in mol m^{-2} s^{-1} was calculated as:

$$R_{vertical} = \frac{\Delta h_i \cdot f_i}{t_2 - t_1} \cdot \frac{1}{V_{mol}} \quad (3)$$

where Δh_i is the change in surface height as measured over the period between t_1 and t_2 at location i, f_i is the i height frequency (see S2 in SI), V_{mol} is the biotite molar volume (140 cm^3 mol^{-1}). The uncertainty generated from the standard deviation of the change in surface height measurements was ≈ 15%.

In oxalic acid solutions, a dissolution rate of pit development (formation and growth) on the basal surface (R_{pit}) was computed by summing the volume loss (V_{loss}) of individual etch pits that developed on the (001) surface over the experimental run. The volume loss was obtained by subtracting a reacted surface from a flat reference surface using a LabView (Laboratory Virtual Instrument Engineering Workbench) routine (see S3 in SI for details). With the moles of dissolved biotite (V_{loss}/V_{mol}), R_{pit} was calculated in mol m^{-2} s^{-1} as:

$$R_{pit} = \frac{V_{loss}}{V_{mol}} \cdot \frac{1}{A*(t_2 - t_1)} \quad (4)$$

where A is the selected surface area. The uncertainty generated from the standard deviation of the change in surface height measurements was ≈ 15%.

The bulk dissolution rate of biotite ($R_{bulk,j}$ in mol m^{-2} s^{-1}) under far-from-equilibrium conditions was obtained by measuring the change in concentration of a component j in solution (j = Si, Al, Mg, Fe and K), defined as:

$$R_{bulk,j} = \frac{1}{\nu_j} \cdot \frac{(C_{j,out} - C_{j,inp})}{m_0 \cdot S} \cdot \frac{V}{dt} \quad (5)$$

where ν_j is the stoichiometric coefficient, $C_{j,out}$ and $C_{j,inp}$ are the concentrations of the output and input solutions of element j, respectively, m_0 is the initial mass, S is the initial biotite BET specific surface area (m^2 g^{-1}), and V is the volume of the batch experiment solution. The uncertainty of the rate was estimated to be about 15-20% according to the propagation method for independent variables (Barrante, 1974), given the 10% and 3% uncertainties from the BET specific surface area measurement and element concentration analyses, respectively.

In the flow-through experiments, the step retreat rate R_{step} in μm s^{-1}) was measured using time resolved LCM-DIM images (Cappelli et al., 2013). R_{step} at a given location of the surface was determined from the horizontal step retreat as:

$$R_{step} = \frac{\Delta L}{(t_2 - t_1)} \quad (6)$$

where ΔL is the change in the surface horizontal length between t_1 and t_2 at a given location. The uncertainty of the rates was estimated to be about 25% (standard deviation calculated from the step retreat values of replicated experiments (Cappelli et al., 2013)).

3. RESULTS AND DISCUSSION

3.1. Biotite dissolution in nitric acid

Ex situ PSI/VSI and in situ LCM-DIM examination of the biotite (001) surface in contact with pH 1-3 nitric acid solutions at 11.5-80 °C (Table 1 and 2) showed that retreat of existing steps over the cleaved surface occurred (Fig. 1). The reaction fronts advanced normal to the step edges, indicating that dissolution of the (hk0) surfaces was taking place. During alteration, swelling and layer peeling were observed at high step fronts (Fig. 1b). Swelling of the basal plane was usually followed by layer cracking. The LCM-DIM measurements of the horizontal step retreat with time allowed us to calculate the step retreat rate (R_{step}, Table 3). Even though preferential formation of etch pits on the biotite (001) surface under acidic conditions has been observed at elevated temperatures (e.g., 120-200 ºC; Pachana et al., 2012; Lamarca-Irisarri et al., 2019), etch pits were not identified at the low pH and temperature ranges of our study. Given the lateral and vertical resolution of the LCM-DIM and VSI techniques, the longest duration of the experiments and the molar volume of biotite, it was deduced that rates of etch pit formation would be lower than 2.8×10^{-12} mol $m^{-2}s^{-1}$.

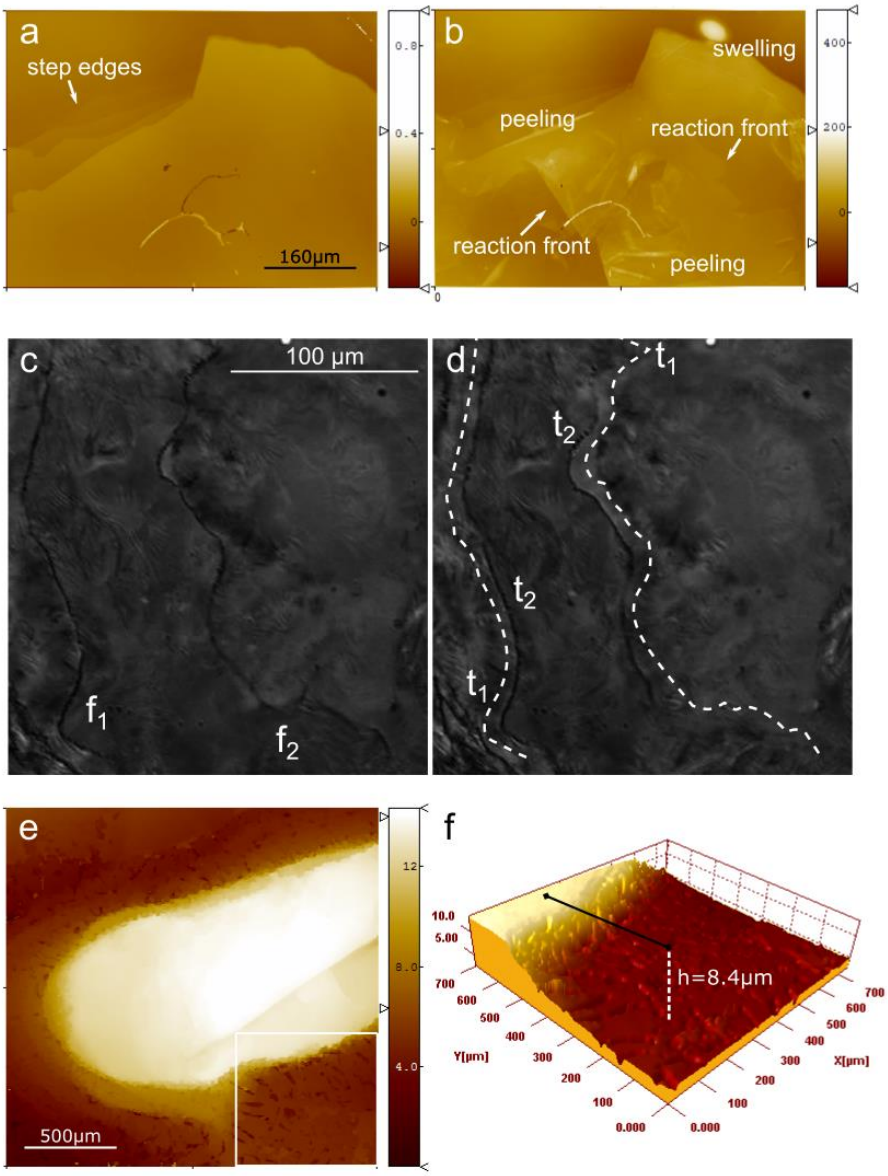

Figure 1. Representative dissolution features of the basal surface of biotite reacted with pH 1 (HNO_3) solution. PSI images of (a) before and (b) after reaction at 25 °C for 48 h (experiment not used for kinetic measurements). LCM-DIM images of a surface reacted at 40 °C for 50 min in a flow-through experiment (c,d) (z scale bar for (a,e) in µm and for (b) in nm). In (d) the dotted lines show previous positions of the dissolution fronts (f_1 and f_2) in (c). The distance measured between the positions of the dissolution fronts at t_1 and t_2 (average value ~10 µm) is used to calculate the step retreat rate. (e) VSI image of unreacted (brightest area) and altered (dark area) biotite surface after 504 h at 40 °C (B2 experiment). The region delimited by the white square in (e) is shown in 3D in (f).

In the batch experiments, $R_{vertical}$ and $R_{bulk,j}$ were obtained for pH 1-3 and for temperatures between 25 and 80 °C (Tables 1 and 3). $R_{vertical}$ corresponds to biotite dissolution at (hk0) surfaces. In turn, $R_{bulk,j}$ was calculated from the cations released from all surfaces (hkl) regardless of the extent of dissolution underwent by different surfaces.

Dissolution took place at a high solution undersaturation with respect to biotite. Solution saturation, expressed as the Gibbs free energy of the reaction, (ΔG_r) was calculated using the EQ3NR code (Wolery, 1992) and the concentrations of the output solutions. ΔG_r ranged from -320 to -371 kJ mol^{-1}. At present, the ΔG_r value at which the biotite dissolution rate is ΔG_r independent is unknown. Given that the muscovite dissolution rate as a function of ΔG_r is independent at $\Delta G_r \approx$ -150 kJ mol^{-1} (Lammers et al., 2017), we assumed that for the calculated ΔG_r range of our experiments, biotite dissolution occurred under far-from-equilibrium conditions.

Based on the $R_{bulk,j}$ values, the reaction stoichiometry was evaluated using R_i/R_{Si} ratios where R_i represents the element bulk rate ($R_{bulk,i}$: R_{Al}, R_{Fe}, R_{Mg} and R_K; Table 3). Biotite dissolution was considered to be stoichiometric when the R_i/R_{Si} ratio was 1 ± 0.2. For the pH range tested, dissolution was stoichiometric with respect to the tetrahedral cations (Al and Si) in 73% of the experiments (Table 3), whereas for the octahedral cations, the Fe and Mg release was stoichiometric in 58% and 46% of the experiments, respectively. Although Kalinowski and Schweda (1996) and Taylor et al. (2000) reported a faster release of octahedral cations compared to tetrahedral Si, which correlated with pH, the non-stoichiometric dissolution observed in our work was either due to an excess or deficit in Fe and Mg regardless the solution pH. Malström and Banward (1997) observed that steady-state dissolution rates were only congruent with respect to Fe, Mg, Al, and Si near pH 2. Pachana et al. (2012) found that the Mg/Si, Fe/Si and Al/Si ratios in solutions were higher compared to ratios in biotite under a temperature range of 120-200 °C and pH range of 1-3.3. As for the exchangeable cation (K), dissolution was mainly non-stoichiometric (85% of the experiments), and both preferential release, as shown by Bray et al. (2014), Malmström and Banwart (1997) and Taylor et al. (2000), and retention (Acker and Bricker, 1992) were observed (Table 3). It has been shown that a switch between release and retention could depend on the degree of Fe(II) oxidation during biotite alteration, which can affect the electrical balance of the structure (Barshad and Kishk, 1968; Gilkes et al., 1972). Moreover, if a mica crystal is cleaved during sample preparation, the (00l) basal face may contain K ions on the tetrahedral sheet, changing the ideal K/Si ratio. In the pH range of 1-3, Al^{3+}, Fe^{2+}, Mg^{2+} and K^+ are the major aqueous species produced during biotite dissolution. Precipitation of secondary Al, Fe and Mg oxy-hydroxide phases is ruled out as a source of deficit in their concentrations given the high solution undersaturation with respect to these phases (Table S1 in Supplementary Information). Kalinowski and Schweda (1996) found that stoichiometric ratios were still far from stoichiometry at the termination of a 2800 h run at pH 2, but they tended towards bulk ratios. The non-stoichiometric release of Fe, Mg > Al > Si for biotite

dissolution in 12 h batch experiments reported by Bray et al. (2015) was, however, not observed in our longer batch experiments with durations of 92-2087 h.

$R_{bulk,Si}$ values were a factor of 12-83 times lower than the $R_{vertical}$ values (Table 3). At 25 °C and pH 1, the obtained $R_{bulk,Si}$ value ($\approx 10^{-10}$ mol m^{-2} s^{-1}) was the same (within error) as that reported by Kalinowski and Schweda (1996) at room temperature using flow-through experiments and biotite powder. At pH 2-3, the $R_{bulk,Si}$ values were about 60-70% faster and 35-68% slower than those reported by Malmström and Banwart (1997) and Bray et al. (2015), respectively, who used powdered samples for their experiments. This rate variability obtained in different laboratories is likely caused by a variety of experimental factors (e.g., choice of minerals and their preparation for experiments, assignment of specific surface areas to the reacting phases (Hodson, 2006), differences in experimental design and length of the experiments (Ullman and Welch, 2002)), and thus limits the reproducibility of dissolution rates of the same mineral. Moreover, the reactivity of millimetric size flakes and powdered samples is different because the grounded grains have a lower basal to edge surface area ratio.

The values of $R_{vertical}$ and $R_{bulk,j}$ rise with increasing temperature and decrease with increasing pH. Likewise, R_{step} rises with temperature at pH 1 (Cappelli et al. (2013); Table 3). These general T and pH-rate trends have been reported for biotite dissolution in organic-free acidic solutions in previous studies (Acker and Bricker, 1992; Turpault and Trotignon, 1994; Kalinowski and Schweda, 1996; Malmström et al., 1996; Malmström and Banwart, 1997; Bray et al., 2015). In sections 3.4 and 3.5 the pH- and T-rate dependencies are discussed in detail.

Table 3. R_{step} (μm s^{-1}), $R_{vertical}$ (mol m^{-2} s^{-1}), $R_{bulk,j}$ (mol m^{-2} s^{-1}) and rate stoichiometry ratios in the presence of HNO_3 acid at different pH.

T (°C)	R_{step}	$R_{vertical}$	$R_{bulk,Si}$	$R_{bulk,Al}$	$R_{bulk,Mg}$	$R_{bulk,Fe}$	$R_{bulk,K}$	R_{Al}/R_{Si}	R_{Mg}/R_{Si}	R_{Fe}/R_{Si}	R_K/R_{Si}
				pH 1							
11.5	7.58E-04										
25	3.80E-03	2.24E-09	1.88E-10	1.86E-10	2.07E-10	2.00E-10	2.10E-10	**1.0**	**1.1**	**1.1**	**1.1**
40	1.90E-02	9.52E-09	4.52E-10	4.29E-10	5.00E-10	4.76E-10	5.00E-10	**0.9**	**1.1**	**1.1**	**1.1**
50	2.60E-02	1.60E-08	1.00E-09	9.29E-10	3.81E-10	1.19E-09	1.40E-09	**0.9**	0.4	**1.2**	1.4
70	6.20eE-2	6.19E-08	3.81E-09	3.81E-09	1.31E-09	3.57E-09	1.67E-09	**1.0**	0.3	**0.9**	0.4
80		1.93E-07									
				pH 2							
25		1.21E-09	6.43E-11	8.33E-11	6.67E-11	8.81E-11	8.81E-11	1.3	**1.0**	1.4	1.4
40		6.19E-09	1.10E-10	1.02E-10	7.38E-11	1.36E-10	7.38E-11	**0.9**	0.7	**1.2**	0.7
40		1.12E-08	1.36E-10	2.10E-10	1.29E-10	1.93E-10	3.33E-10	1.5	**0.9**	1.4	2.5
50		1.83E-08	2.62E-10	3.33E-10	3.81E-10	9.76E-11	1.50E-10	1.3	1.5	0.4	0.6
50		1.14E-08	4.29E-10	4.52E-10	4.76E-10	5.71E-10	5.48E-10	**1.1**	**1.1**	1.3	1.3
70		2.62E-08	6.67E-10		4.76E-11	5.24E-10	1.38E-11		0.1	**0.8**	0.0
				pH 3							
25		4.29E-10	1.93E-11	2.10E-11	7.86E-11	2.26E-11	5.48E-11	**1.1**	4.1	**1.2**	2.8

40	9.76E-10	6.19E-11	7.38E-11	5.95E-11	6.43E-11	8.81E-11	**1.2**	**1.0**	**1.0**	1.4
70	4.76E-09	1.07E-10		1.45E-10		2.86E-11		1.4		0.3

R_i/R_j in bold indicates stoichiometric biotite dissolution (within 20%).

3.2 Biotite dissolution in oxalic acid

In the batch experiments, ex-situ VSI observations of the biotite (001) surface showed that in the presence of oxalic acid (pH 1.3 and 2.1) at 25-70 ºC dissolution was controlled by the formation and growth of etch pits and to a lesser extent by the edge retreat of preexisting steps (Fig. 2). Etch pits showed a round shape and homogeneous size and were distributed all over the surfaces inspected (Fig. 2a-d). The step edges were characterized by irregular dissolution contours (Fig. 2e). At the highest temperature (70 ºC), the etch pits expanded fast and merged, yielding a significant surface roughening (Fig. 2d). For instance, the root mean square roughness (R_q) increased from 4.4 nm at 50 ºC to 20 nm at 70 ºC (details in SI).

The extensive etching of the basal surface took place at a solution undersaturation that was considerably higher than that in the oxalic-free solutions, i.e. ΔG_r values ranged from -547 to -577 kJ mol^{-1}. Speciation calculations of the output solutions at 25 °C and 0.1 M oxalic acid using EQ3 (Wolery, 1992) show that at pH values of 1.3 and 2.1, formation of aqueous Fe-, Al- and Mg-oxalate complexes reduced the concentrations of free aqueous Fe, Al and Mg, resulting in a higher solution undersaturation. This high degree of undersaturation with respect to biotite exposes the basal surface to a free energy regime in which significant reactive topography (i.e., etch pits) develops (Lüttge et al., 2019). In oxalic-free solutions, ΔG_r ranged from -320 to -371 kJ mol^{-1}. This ΔG_r interval falls in a far-from-equilibrium region, in which the undersaturation condition reached should be sufficient for hollow cores to open up (Lasaga and Luttge, 2001; Lüttge et al., 2019). However, etch pits were not observed under our experimental conditions and VSI resolution. Etch pits were only observed at the higher degree of undersaturation with respect to biotite in oxalic solutions. As a matter of fact, an increase in the concentration of oxalic acid along with an associated reduction in the concentration of free cations involved in the reaction thereby, resulted in a significant increase in etch pit density (Fig. 2c,d).

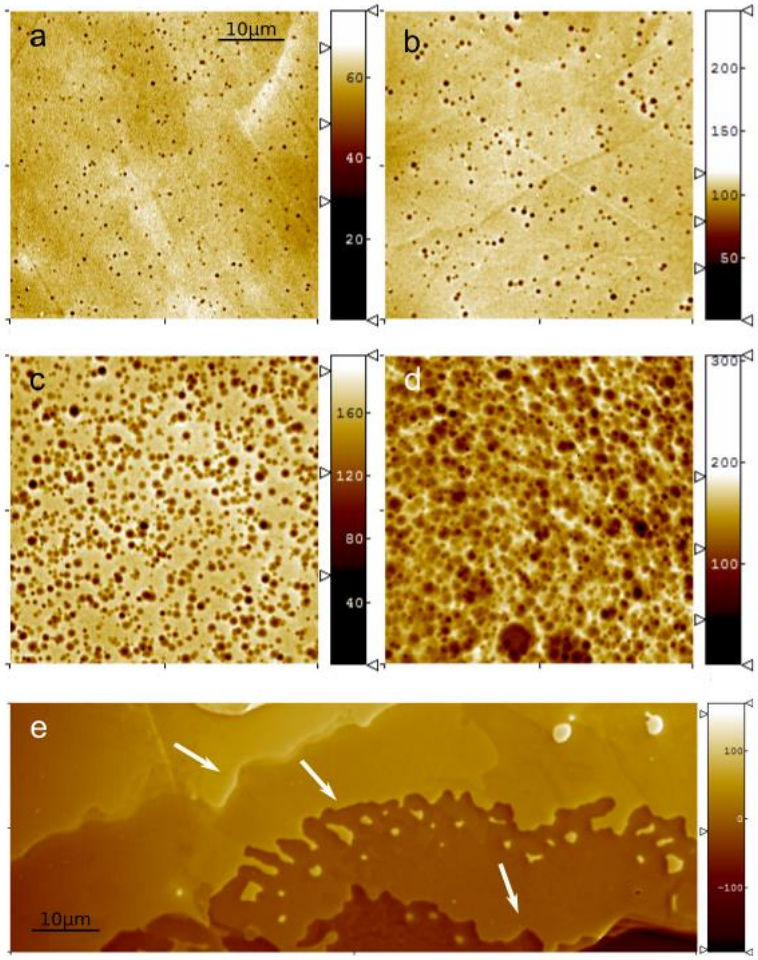

Figure 2. VSI images of reacted biotite (001) surface with oxalic acid at: (a) 50 °C with 0.1 M solution for 72 h [experiment B4ox]; (b) 50 °C with 0.1 M solution for 191 h [experiment B5ox]; (c) 70 °C with 0.01 M solution for 72 h [experiment B12ox]; (d) 70 °C with 0.1 M solution for 192 h [experiment B6ox]; (e) 50 °C with 0.01 M solution for 72 h [experiment B9ox]. Same x-y scale bar in (a-d) images; z scale bar in nm (a-e). White arrows in (e) show highly dissolved step edges with irregular contours.

Bulk dissolution rates ($R_{bulk,Si}$, $R_{bulk,Al}$, $R_{bulk,Mg}$ and $R_{bulk,K}$) and basal pit dissolution rates (R_{pit}) are listed in Table 4. Similar to the oxalate-free solutions, $R_{bulk,i}$ values were obtained from the cations released in solution from dissolving (hkl) surfaces, whereas R_{pit} was the rate associated with etch pit development on the (001) surface. In oxalic solutions, LCM-DIM could not be used to quantify the horizontal step retreat because the high irregular contours of dissolving edges (Fig. 2e) made reliable measurements of dissolution-front distances over time impossible.

Biotite dissolution was stoichiometric (i.e. R_i/R_{Si} ratio = 1 ± 0.2) with respect to the tetrahedral cations in 63% of the experiments at both pH values (1.3 and 2.1; Table 4). In the case of non-stoichiometric experiments (37%), Al was released faster than Si. As for the octahedral cations, the R_{Mg}/R_{Si} ratio was between 0 and 0.2, indicating a substantial deficit in

aqueous Mg. In contrast, R_{Fe}/R_{Si} was approximately stoichiometric. The exchangeable cation (K) showed a slow release ($R_K/R_{Si} < 1$), likely controlled by diffusion (Malmström and Banwart, 1997; Taylor et al., 2000), but with a deficit smaller than that of Mg.

Regarding Mg depletion, Rozalen and Huertas (2013) observed the formation of Mg-oxalate solid phases (e.g., glushinskite ($Mg(C_2O_4)\cdot 2H_2O$)) after organic ligand complexation during chrysotile dissolution at 25 °C and pH ≈ 1.5. This process could account for both the lack of aqueous Mg and formation of precipitates on the basal surface, which was observed during dissolution (Fig. 3). Unfortunately, the micro-precipitates could not be identified to confirm this hypothesis.

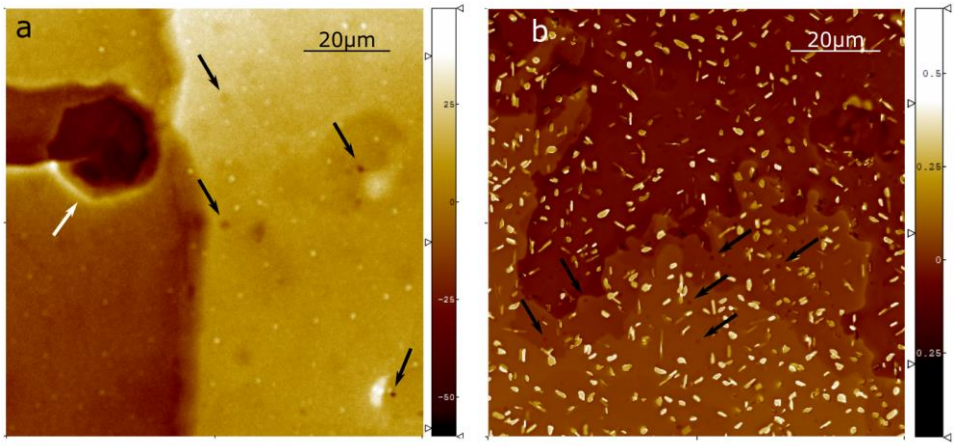

Figure 3. VSI image of biotite (001) surface after reaction at 40 °C with 0.1 M oxalic acid for (a) 24 h and (b) 120 h (experiment not used for kinetic measurements); z scale bar for (a) and (b) in nm and µm, respectively. Small precipitates (white spots in (a)) formed after 24 h and grew with time (b). Note that, despite the abundant precipitation, etch pits (pointed out by black arrows) kept forming on the surface. White arrow in (a) points out a wide hexagonal pit that likely originated at surface defects.

As with biotite dissolution in nitric acid solutions, $R_{bulk,j}$ and R_{pit} in oxalic acid solutions increased with rising temperature and decreasing pH (Table 4). The temperature effect on the reactivity of the (001) surface was perceptible by comparing the etch pit evolution in 0.01-0.1 M oxalic acid solutions between 50 and 70 °C for the same surface area (Figs. 2a-d). At 50 °C and pH 1.3, the etch pit density remained nearly constant after 191 h (≈ 0.17 etch pit μm^2) with an increase in the etch pit size (Fig. 2a,b), suggesting that etch pit growth (step spread) was faster than etch pit nucleation (deepening). At 70 °C, pH 1.3 and same reaction time (Fig. 2b,d), a faster pit nucleation resulted in a higher pit density (≈ 0.5 etch pit μm^2), and faster growth led to pit merging, thereby yielding a highly altered basal surface (Fig. 2d).

Table 4. R_{pit}, $R_{bulk,j}$ (mol m^{-2} s^{-1}) and rate stoichiometry ratios in the presence of $H_2C_2O_4$ acid at pH 1.3 (0.1 M $H_2C_2O_4$) and pH 2.1 (0.01 M $H_2C_2O_4$).

T (°C)	R_{pit}	$R_{bulk,Si}$	$R_{bulk,Al}$	$R_{bulk,Mg}$	$R_{bulk,Fe}$	$R_{bulk,K}$	R_{Al}/R_{Si}	R_{Mg}/R_{Si}	R_{Fe}/R_{Si}	R_K/R_{Si}
				pH 1.3						
25	4.52E-12	8.57E-11	1.12E-10	1.83E-11	7.86E-11	4.52E-11	1.3	0.2	**0.9**	0.5
40	3.57E-11	2.62E-10	2.62E-10	4.05E-11	2.31E-10	1.24E-10	**1.0**	0.2	**0.9**	0.5
50	8.57E-10	5.24E-10	4.52E-10	5.71E-11	4.05E-10	2.38E-10	**0.9**	0.1	**0.8**	0.5
70		1.69E-09	2.62E-09	4.05E-10	1.50E-09	1.95E-09	1.5	0.2	**0.9**	**1.2**
				pH 2.1						
25		6.19E-11	6.67E-11	5.48E-13	7.14E-11		**1.1**	0.0	**1.2**	
40	2.31E-11	1.55E-10	1.79E-10	5.00E-12	1.55E-10		**1.2**	0.0	**1.0**	
50	5.24E-11	2.02E-10	3.81E-10	2.14E-11	1.76E-10	2.62E-11	1.9	0.1	**0.9**	0.1
50	6.19E-11									
70	1.17E-09	4.05E-10	3.81E-10	7.62E-11			**0.9**	0.2	**0.8**	**0.9**

R_i/R_{Si} in bold indicates stoichiometric biotite dissolution (within 20%).

3.3. The effect of oxalic acid on the biotite dissolution rate

Our experimental results show that the development of etch pits in the presence of oxalic acid strongly degrades the basal surface. As shown by Haward et al. (2011), the formation of pits will expose (hk0) surfaces to both proton and ligand attack, resulting in rapid etch pit growth relative to the etch pit formation. At pH ≤ 3 the main process responsible for the intense degradation of biotite surface must be the capacity of the organic ligand to form inner-sphere surface complexes involving both carboxyl groups of the oxalic acid (single protonated (HOx^-) and fully deprotonated (Ox^{2-})) with tetrahedral (>AlOH and >$AlOH_2^+$) and octahedral (>Mg-FeOH and >Mg-$FeOH_2^+$) edge surface sites (Ganor et al., 2009). These processes have been studied at the molecular level for feldspar dissolution in oxalic acid (pH 0-6) by molecular dynamic simulations (Xue et al., 2019). It was demonstrated that dissolution is promoted by the complex reaction between >Al surface sites and H_2O, H_2Ox, HOx^- and Ox^{2-}, and protons (H^+) attacking the >Si surface site. At very low pH, $H_2C_2O_4$ forms outer-sphere complexes with >Al active sites. As pH increases, $HC_2O_4^-$ and $C_2O_4^{2-}$ attack Al active site (inner-sphere adsorption) promoting Al release. In the acid pH range, H^+ attacks Si to promote Si release.

Ganor et al. (2009) defined the enhancement ratio as the ratio between dissolution rate with organic matter and dissolution rate without organic acids (for the same temperature and pH). Based on a number of studies on the effect of oxalic acid on dissolution of aluminosilicates, it has been shown that the enhancement ratio can be up to 10 (e.g., Zhang and Jun, 2015), but is usually less than 3 with a median value of only 2, indicating that the catalytic effect of oxalate is generally relatively small. In our experiments with $H_2C_2O_4$ (pH 1.3 and 2.1; Fig. 2), despite the remarkable degradation of the basal surface observed, the respective bulk dissolution rates are about 30% lower or nearly equal to those measured without oxalate (Table 5), yielding averaged enhancement ratios ($R_{bulk,H2C2O4}/R_{bulk,HNO3}$) of 0.7

± 0.1 (pH = 1.3) and 1.1 ± 0.5 (pH = 2.1), respectively, over the temperature range of 25-70 °C (Table 5). Note that to calculate the enhancement ratios at pH 1.3 and 2.1, the $R_{bulk,HNO3}$ values were re-calculated from the values obtained at pH 1 and 2 using a proton reaction order (n_{H+}) of 0.46 (see section 3.4 and Eq. (1)).

Table 5. $R_{bulk,Si}$ values and enhahncement ratios obtained for oxalic and nitric acid solutions.

T (°C)	$R_{bulk,Si}$ ($H_2C_2O_4$)	$R_{bulk,Si}$ (HNO_3)	enhancement ratio ($R_{bulk,H2C2O4}/R_{bulk,HNO3}$)
pH 1.3			
25	8.6E-11	1.4E-10	0.6
40	2.6E-10	3.3E-10	0.8
50	5.2E-10	6.7E-10	0.8
70	1.7E-9	2.3E-9	0.7
pH 2.1			
25	6.2E-11	5.5E-11	1.1
40	1.5E-10	1.5E-10	1.0
50	2.0E-10	2.3E-10	0.9
70	4.1E-10	5.4E-10	0.7

Drever and Stillings (1997) argued that the effect of oxalate on silicate dissolution becomes significant at total oxalate concentration of ≈ 0.001 M, and Golubev et al. (2006) showed that concentrations of organic ligands in the range of 0.01-0.1 M were required to increase the smectite dissolution rate by a factor of 3 at circum-neutral pH. Even though the concentration of oxalic acid (ligand) matched the required range in the study herein, the catalytic effect expected on the bulk dissolution rates was not observed. This finding, on the one hand, suggests that under high acidity conditions (pH 1.3-2.1) the contribution of H^+ attacking > Si sites to the overall rate is larger than that of the ligand attacking >Al sites (i.e., outer-sphere adsorption of H_2Ox and inner-sphere adsorption of HOx^- on >Al surface sites; see Fig. 19 in Xue et al., 2019). This is consistent with the results of Balland et al. (2010) and Bray et al. (2015) who reported a negligible effect on Si release during biotite dissolution in the presence of citric and gluconic acid (10^{-3}-10^{-2} M) and oxalic acid ($5 \cdot 10^{-4}$ M) at pH < 3. Only at pH of 3 or above did the presence of the organic ligand increase the element release relative to the ligand-free experiments.

On the other hand, one would expect that the increase in basal degradation observed in the presence of oxalic acid renders an increase in the bulk dissolution rates. However, the lack of enhancement of the dissolution rate does not imply the lack of an incipient contribution of the basal etch pits to the bulk dissolution rate. After the early dissolution stage

during which etch pits form and hollow cores stabilize the bulk dissolution rate is mainly determined by the retreat of step edges and is only slightly dependend on the etch pit nucleation rate (Luttge et al., 2019).

In general, our experimental data show that the contribution of the basal plane etching to the overall dissolution rate increases with temperature. Taking into account the dimensions of the flakes and assuming them to have a parallelepiped shape with flat surfaces, the basal and lateral surfaces account for a respective ≈ 85-90 % and ≈ 10-15% of the total surface. Considering that edge surfaces dissolve 120 to 250 faster than basal surfaces of biotite in ligand-free solutions (Turpault and Trotignon, 1994; Bray et al, 2015), the contribution of the edge surface to the bulk dissolution rate is still 12 to 25 times higher than the basal surface (i.e. $R_{bulk,Si}/R_{pit}$ ratio > 12-25). Nevertheless, this assumption is only confirmed at lower temperatures, for which the $R_{bulk,Si}/R_{pit}$ ratio is 20 (25 ºC) and 7 (40 ºC) at pH 1.3 and 7 (25 ºC) and 4 (40 ºC) at pH 2.1. At 50 and 70 ºC, the ratio is 0.6 and 0.4, respectively, indicating that a rise in temperature induces a noticeable increase in the pit basal rate ($R_{pit} > R_{bulk,Si}$).

3.4. The effect of pH on the biotite dissolution rate

The effect of pH on the dissolution rate of biotite in the HNO_3 solutions was determined for a range of pH (1-3) and a range of temperature (25-70 °C) (Fig. 4). It was assumed that the rate ($Rate_{H+}$) is proportional to a fractional power of the proton activity as expressed in the first term of Eq. (1) as:

$$Rate_{H^+} = k_{H^+} \cdot a_{H^+}^{n_{H^+}} \quad (7)$$

where the proportionality constant (k_{H+}) is calculated based on $R_{vertical}$ and $R_{bulk,Si}$ at different pH and temperature, a_{H+} is the proton activity in solution and n_{H+} is the proton reaction order. The values listed in Table 6 show that according to the variation in $R_{vertical}$, n_{H+} increases with increasing temperature from 0.36 (25 °C) to 0.56 (70 °C). Variation in $R_{bulk,Si}$ yields n_{H+} values that are similar (within error) at 25, 40 and 50 °C (0.49, 0.43 and 0.58, respectively) and higher at 70 °C (0.77).

Previous dissolution studies using biotite powdered samples at 22-25 °C showed that biotite dissolves faster at the edges than on basal surfaces (e.g., Turpault and Trotignon, 1994). Under acid conditions, the reaction orders obtained from the bulk dissolution rates ranged from 0.31 to 0.91 depending on the surface area used to normalize the rates and the selection of the element released (Table 6): 0.34 ($3 \leq pH \leq 7$; Acker and Bricker (1992); 0.35-0.61 ($1 \leq pH \leq 4$; Kalinowski and Schweda, 1996); 0.40-0.91 ($2 \leq pH \leq 7$; Malmström and Banwart, 1999); 0.31-0.58 ($2 \leq pH \leq 6$; Bray et al., 2015). Given the similarity of our values to these prior studies (Fig. 4), it is reasonable to assume that the bulk and vertical rates

primarily describe dissolution driven by step edge retreat. At 70 °C, the n_{H+} values are slightly higher (0.56 ($R_{vertical}$) and 0.77 ($R_{bulk,Si}$)), but still fall within the range of n_{H+} at room temperature reported in the previous studies (Table 6).

Bray et al. (2014) demonstrated that the surface reactivity of biotite changes with pH and that the concentration of protons consumed ($[H_s^+]$) by biotite in contact with acid solutions (pH < 4) at 25 °C is subject to the concentrations of protons consumed by biotite dissolution ($[H_{dis}^+]$), hydrolysis of aqueous cations ($[H_{hy}^+]$), metal exchange reactions ($[H_{ex}^+]$) and proton adsorption ($[H_{ad}^+]$), i.e., $[H_s^+] = [H_{diss}^+] + [H_{hy}^+] + [H_{ex}^+] + [H_{ad}^+]$). The study showed that the surface of biotite is predominantly composed of Si at pH < 3 and that the adsorption of H^+ ($[H_{ad}^+]$) forms partly detached silanol groups. It is reasonable, therefore, to assume that this mechanism characterizes the biotite PPRM over the low pH range used in this study. Under this highly acidic condition, the n_{H+} value of 0.46 ± 0.03 is proposed as an average proton reaction order over the T range of 25-50 °C. The variability of n_{H+} observed in the prior studies (Table 6), performed over a broader acid pH range of 1-7, is likely due to the decrease in silanol detachment in favor of an increase in the detachment of aluminol groups and iron and magnesium octahedral groups at pH above 3 (Xue et al., 2019). At higher temperatures (e.g., 70 °C), however, the reactions involved (e.g., proton exchange and adsorption) may be either catalyzed or shifted to result in greater reaction order values (e.g., n_{H+} = 0.56 and 0.77).

Table 6. Proton reaction orders (n_{H+}) and proportional constants (k_{H+}) calculated using $R_{vertical}$, R_{pit} and $R_{bulk,Si}$ at pH range = 1-3 (Table 3) and at pH range = 1-7 (other studies).

acid	T	$k_{H+}(R_{vertical})$	$n_{H+}(R_{vertical})$	$k_{H+}(R_{bulk,Si})$	$n_{H+}(R_{bulk,Si})$
HNO_3	25	$10^{-8.3}$	0.36 ±0.05	$10^{-9.2}$	0.49 ±0.01
	40	$10^{-7.4}$	0.49±0.01	$10^{-8.9}$	0.43 ±0.10
	50	n.d.	n.d.	$10^{-8.6}$	0.45 ±0.15
	70	$10^{-6.6}$	0.56 ±0.04	$10^{-7.6}$	0.77 ±0.03
	22			$10^{-10.0}$	0.34[(1)]
	25			$10^{-9.8}$	0.35-0.61 [(2)]
	25			$10^{-8.0}$	0.40-0.91[(3)]
	25			$10^{-9.1}$	0.31-0.58[(4)]
$H_2C_2O_4$	25				0.19 ±0.04
	40		0.22 ±0.04		0.25 ±0.05
	50		1.46 ±0.30		
	70				0.76 ±0.20

[(1)]pH range = 3-7; Acker and Bricker (1992); [(2)]pH range = 1-4; Kalinowski and Schweda (1996); [(3)]pH range = 2-7; Malmström and Banwart (1997); [(4)]pH range = 2-6; Bray et al. (2015); n.d. = no data.

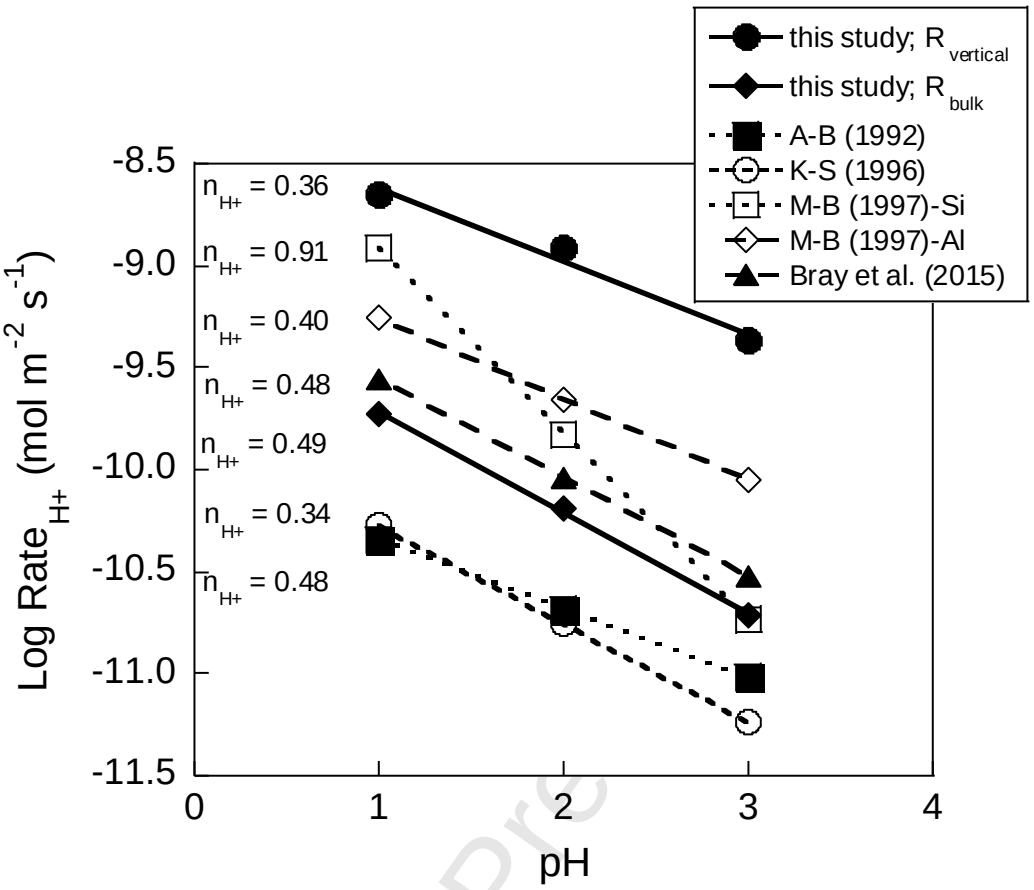

Figure 4. Plot of the logarithm of the dissolution rate ($Rate_{H+}$) as a function of pH to calculate the proton reaction orders at room T (22-25 °C) for this study and previous studies. Note that with the exception of $R_{vertical}$, the values of the surface area normalized rates depend on the element release (Si or Al) as shown in the legend. A-B (Acker and Bricker,1992); K-S (Kalinowski and Schweda,1996); M-B (Malmström and Banwart, 1997); Bray et al.,2015).

Estimates of the overall dissolution rate dependence on pH in the presence of $H_2C_2O_4$ at pH = 1.3 and 2.1 were carried out using the respective $R_{bulk,Si}$ ($n_{H+} \approx 0.20$ at 25-40 °C and ≈ 0.76 at 70 °C) and R_{pit} values ($n_{H+} \approx 0.20$ at 40 °C and ≈ 1.46 at 50 °C; Table 6). Assuming that proton adsorption on biotite is independent of oxalate adsorption (i.e. PPRM and OPRM are independent mechanisms) and the former mechanism is not affected by the adsorption of oxalate, n_{H+} should not change in acid/ligand solutions. The resulting n_{H+} variation with respect to the inorganic solutions at lower temperatures, i.e., $n_{H+} \approx 0.20$ in $H_2C_2O_4$ and $n_{H+} \approx 0.49$ in HNO_3 for 25-40 °C, is therefore unexpected. The elevated n_{H+} value of 1.46 at 50 °C is likely caused by the effect of step density on R_{pit} at different temperatures as explained in the next section. Nevertheless, to account for this discrepancy further experimental investigation and biotite molecular dynamic simulations are warranted.

3.5. The effect of temperature on the biotite dissolution rate

In the HNO_3 solutions, the apparent activation energy of the dissolution reaction (E_a) was calculated using the Arrhenius law:

$$R_{H+} = A \cdot e^{\frac{-E_{a;H+}}{RT}} \quad (8)$$

where A is a pre-exponential factor, R is the gas constant and T is the temperature (K).

The E_a values derived from $R_{vertical}$ and $R_{bulk,Si}$ range from 31 (pH = 3) to 63 kJ mol^{-1} (pH = 1) (Fig. 5a,b), and the latter value is the same (within error) as that obtained from R_{step} (E_a = 62 kJ mol^{-1}) (Table 7). This variability, whereby E_a decreases by lowering acidity and that E_a derived from $R_{bulk,Si}$ is systematically higher than that from $R_{vertical}$, is not surprising because the pH effect on the dissolution rate is controlled by protons adsorbed on the surface and not directly from the solution pH (e.g., [H_s^+]; Bray et al., 2014). Therefore, performing the experiments at the same pH is not enough to keep the pre-exponential factor (A) in Eq. (8) constant in all cases. Within this respect, it is probable that the surface coverage of protons varied with temperature, i.e., protonation-deprotonation of biotite surface sites could be temperature dependent, as was shown to occur for kaolinite by Cama et al. (2002). As a consequence, the dissolution rates at the same pH and different temperature are influenced by different proton concentrations on the surface. In the present study, the contribution of the involved surface reactions (hydrolysis of aqueous cations, metal exchange and proton adsorption) on the total proton consumption, i.e., the proton coverage dependence with pH and temperature, remains unknown. Hence, until the dependence of the surface coverage of protons on pH and temperature is known for biotite, we propose the average E_a value of 62 ± 9 kJ mol^{-1}, derived from R_{step}, $R_{vertical}$ and $R_{bulk,Si}$ at pH = 1, to account for the dissolution rate-temperature dependence at acidic pH. Yet the E_a values calculated from $R_{vertical}$ and $R_{bulk,Si}$ are the same within uncertainty at the pH range of 1-2 and slightly lower at pH 3 (Table 7).

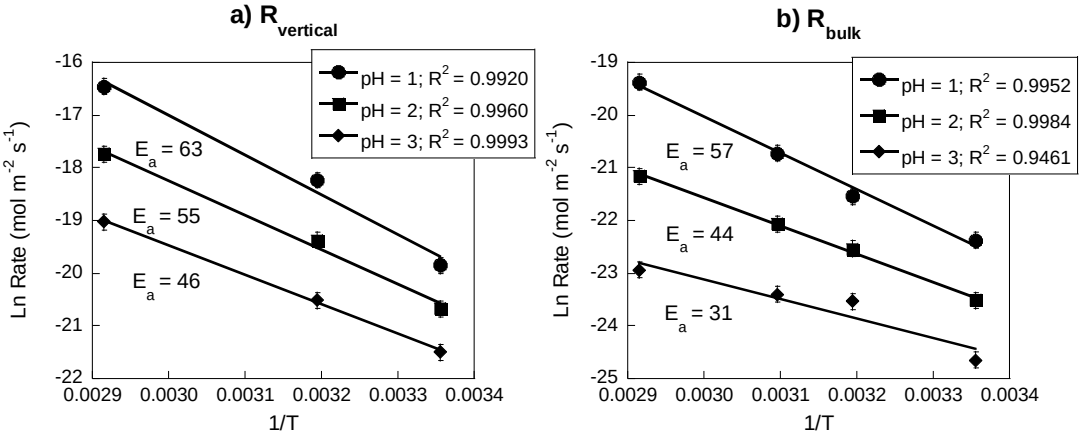

Figure 5. Arrhenius plots (ln dissolution rate ($Rate_{H+}$) as a function of 1/T) at pH = 1, 2 and 3 to calculate E_a (kJ mol^{-1}): a) from R_{vertical} variation and b) from $R_{\text{bulk,Si}}$ variation.

The results showed that highly acidic solutions with 0.01 and 0.1 M concentrations of $H_2C_2O_4$ were enough undersaturated to prompt pit nucleation and growth on the (001) surface but could not enhance the measured inorganic dissolution rates (Table 5). The organic rate-based values were slithgly lower (E_a = 56 kJ mol^{-1} (pH = 1.3) and 36 kJ mol^{-1} (pH 2.1)) and decreased with increasing pH when derived from $R_{bulk,Si}$ and much higher (E_a = 121 and 162 kJ mol^{-1} (pH 2.1 and 1.3)) when derived from R_{pit} (Table 7).

Table 7. E_a (kJ mol^{-1}) values calculated from R_{step}, $R_{vertical}$, R_{pit} and $R_{bulk,Si}$ at different pH.

Acid	pH	E_a from R_{step} (LCM-DIM)	E_a from $R_{vertical}$, R_{pit} (VSI, PSI)	E_a from $R_{bulk,Si}$ (bulk analysis)	$^{(1)}E_a$ from $R_{pit\ growth}$ (AFM)	$^{(1)}E_a$ from $R_{pit\ formation}$ (AFM)
Nitric acid	1	62±9	63±4	57±5		
	2		55±5	46±6		
	3		46±3	31±8		
Oxalic acid	1.3		162±14 **(001)**	56±2	49±2	40 -140 **(001)**
	2.1		121±33 **(001)**	36±2		

$^{(1)}$Haward et al. (2011) using in situ real-time AFM imaging; **(001)** indicates values associated with etch pit formation otherwise correspond to (hk0) surface.

The high E_a values derived from R_{pit} calculations represent dissolution of combined etch pit formation (deepening) and pit growth (step spread). These values are very similar to the value that Haward et al. (2011) obtained from the slow formation of etch pits at a low step density on the basal surface with the same oxalate concentration (140 kJ mol^{-1};Table 7). The study found that as etch pits evolved and step density increased, E_a decreased to a value of 40 kJ mol^{-1}. This trend is consistent with the step wave model described in Lasaga and Luttge (2001) that predicts a decrease in the etching contribution to the overall dissolution, as steps spread from etch pits leading to a coalescence of etch pits. The E_a value that was derived by Haward et al. (2011) to represent dissolution of (hk0) surfaces is similar to the value we obtained both in the absence and in the presence of oxalic acid (E_a = 49 ± 2, 57 ± 5 and 56 ± 2 kJ mol^{-1}, respectively; Table 7).

Conclusions

The dissolution kinetics of biotite were studied in nitric acid (HNO_3) and oxalic acid ($C_2H_2O_4$) solutions under far-from-equilibrium over a temperature range of 11.5-80 °C. An analysis of the aqueous chemistry was used to calculate bulk dissolution rates, whereas high-resolution microscopy techniques (VSI/PSI and LCM-DIM) were used to derive surface dissolution rates from topography measurements (vertical and horizontal dissolution rates (step retreat) and basal mass loss by etch pit development).

In the presence of nitric acid (pH range of 1-3), retreat of (hk0) steps controlled biotite dissolution, while the formation of etch pits were not detected within the experimental time frames and the VSI resolution. By contrast, in the presence of oxalic acid (0.01-0.1 M) at a higher degree of undersaturation, basal etch pits developed.

In the absence and in the presence of oxalic acid, the biotite dissolution was not always stoichiometric, and there was no specific correlation between pH, the release of the structural elements and/or the presence of oxalate. When dissolution is nonstoichiometric, there was a preferential release of tetrahedral Al and octahedral Fe and Mg over tetrahedral Si, although in the presence of oxalate, Fe release was stoichiometric and Mg released may precipitate as glushinkite. The release of the interlayer cation, K, was subject to relatively fast cation exchange, diffusion, and Fe(II) oxidation during biotite alteration.

In oxalic-free solutions, for the ranges of pH and temperature studied in this work, the proton reaction order (n_{H+}) increases with temperature (from 0.46 to 0.77) and the apparent activation energy ($E_{a;H+}$) decreases with pH from 63 to 31 kJ mol^{-1}. These findings denote the importance of evaluating the different processes involved in the proton consumption during mineral dissolution as a function of temperature and pH in order to model proton surface adsorption and thereby the dissolution kinetics.

At very acidic conditions (pH 1-3) with oxalic acid, the PPRM rate dominates over the OPRM rate, suggesting that the ligand effect (i.e., inner-sphere HOx^-- and Ox_2^- ->Al site coordination) on the overall rate is small and that proton adsorption (i.e., H^+ attacking Si site) dominates over oxalate adsorption. Moreover, an increase in temperature, induces an increase in R_{pit} (basal dissolution rate) compared with the $R_{bulk,Si}$ (bulk dissolution rate). This observation togheter with the higher E_a values (121 and 162 kJ mol^{-1}) found for R_{pit} rates indicates a strong temperature effect on the etch pit formation. Despite the small impact of the OPRM on the overall dissolution rate, n_{H+} and E_a become smaller in the presence of oxalate

($n_{H+} \approx 0.20$ and $E_{a,ox} \approx 50$ kJ mol^{-1}), suggesting that OPRM slightly contributes to enhance biotite dissolution.

Acknowledgement

This work was supported by the CGL2011–22567, CGL2014–55108-P, CGL2016–78783–C2-R, CGL2017–82331-R and CEX2018–000794-S projects (Spanish Ministry of Science and Innovation) with contribution of FEDER funds and the Catalan Government through project 2017SGR 1733. AESVD acknowledges funding from the CNRS IEA program (PICS07954). CC benefited from a Spanish Ministry of Education grant. We wish to thank Dr. Luis D. Patiño-López for assistance in VSI/PSI data acquisition. We thank Felix Brandt, one anonymous reviewer and the Editor, Michael E. Böttcher, for their thorough reviews that significantly improved the quality of the manuscript.

References

Acker, J.G., Bricker, O.P., 1992. The influence of pH on biotite dissolution and alteration kinetics at low temperature. Geochimica et Cosmochimica Acta, 56(8): 3073-3092.

Aldushin, K., Jordan, G., Aldushina, E., Schmahl, W.W., 2007. On the kinetics of ion exchange in phlogopite: an in situ AFM study. Clays and Clay Minerals, 55(4): 339-347.

Aldushin, K., Jordan, G., Rammensee, W., Schmahl, W.W., Becker, H.-W., 2004. Apophyllite (001) surface alteration in aqueous solutions studied by HAFM. Geochimica et Cosmochimica Acta, 68(2): 217-226.

Aldushin, K., Jordan, G., Schmahl, W.W., 2006. Basal plane reactivity of phyllosilicates studied in situ by hydrothermal atomic force microscopy (HAFM). Geochimica et Cosmochimica Acta, 70(17): 4380-4391.

Amram, K., Ganor, J., 2005. The combined effect of pH and temperature on smectite dissolution rate under acidic conditions. Geochimica et Cosmochimica Acta, 69(10): 2535-2546.

Arvidson, R.S., Ertan, I.E., Amonette, J.E., Luttge, A., 2003. Variation in calcite dissolution rates:: A fundamental problem? Geochimica et Cosmochimica Acta, 67(9): 1623-1634.

Barrante J. (1974) Applied mathematics for physical chemistry. Englewood Cliffs, New Jersey.

Balland, C., Poszwa, A., Leyval, C., Mustin, C., 2010. Dissolution rates of phyllosilicates as a function of bacterial metabolic diversity. Geochimica et Cosmochimica Acta, 74(19): 5478-5493.

Barshad, I., Kishk, F.M., 1968. Oxidation of Ferrous Iron in Vermiculite and Biotite Alters Fixation and Replaceability of Potassium. Science, 162(3860): 1401-1402.

Bauer, A., Berger, G., 1998. Kaolinite and smectite dissolution rate in high molar KOH solutions at 35° and 80°C. Applied Geochemistry, 13(7): 905-916.

Bickmore, B.R., Bosbach, D., Hochella, M.F., Jr., Charlet, L., Rufe, E., 2001. In situ atomic force microscopy study of hectorite and nontronite dissolution: Implications for phyllosilicate edge surface structures and dissolution mechanisms. American Mineralogist, 86(4): 411-423.

Brandt, F., Bosbach, D., Krawczyk-Bärsch, E., Arnold, T., Bernhard, G., 2003. Chlorite dissolution in the acid ph-range: a combined microscopic and macroscopic approach. Geochimica et Cosmochimica Acta, 67(8): 1451-1461.

Brantley, S.L., 2008. Kinetics of Mineral Dissolution. In: Brantley, S.L., Kubicki, J.D., White, A.F. (Eds.), Kinetics of Water-Rock Interaction. Springer, NewYork, pp. 151-210.

Bray, A.W., Benning, L.G., Bonneville, S., Oelkers, E.H., 2014. Biotite surface chemistry as a function of aqueous fluid composition. Geochimica et Cosmochimica Acta, 128(0): 58-70.

Bray, A.W. et al., 2015. The effect of pH, grain size, and organic ligands on biotite weathering rates. Geochimica et Cosmochimica Acta, 164: 127-145.

Cama, J., Ganor, J., 2006. The effects of organic acids on the dissolution of silicate minerals: A case study of oxalate catalysis of kaolinite dissolution. Geochimica et Cosmochimica Acta, 70(9): 2191-2209.

Cama, J., Ganor, J., 2015. Chapter 4 - Dissolution Kinetics of Clay Minerals. In: Tournassat, C., Steefel, C.I., Bourg, I.C., Bergaya, F. (Eds.), Developments in Clay Science. Elsevier, pp. 101-153.

Cama, J., Ganor, J., Ayora, C., Lasaga, C.A., 2000. Smectite dissolution kinetics at 80°C and pH 8.8. Geochimica et Cosmochimica Acta, 64(15): 2701-2717.

Cama, J., Metz, V., Ganor, J., 2002. The effect of pH and temperature on kaolinite dissolution rate under acidic conditions. Geochimica et Cosmochimica Acta, 66(22): 3913-3926.

Cappelli, C., Lamarca-Irisarri, D., Cama, J., Huertas, F.J., Van Driessche, A.E., 2015. In situ observation of biotite (001) surface dissolution at pH 1 and 9.5 by advanced optical microscopy. Beilstein journal of nanotechnology, 6(1): 665-673.

Cappelli, C., Van Driessche, A.E.S., Cama, J., Huertas, F.J., 2013. In Situ Observation of Biotite Dissolution at pH 1 Using Advanced Optical Microscopy. Crystal Growth & Design, 13(7): 2880-2886.

Cappelli, C., Yokoyama, S., Cama, J., Huertas, F.J., 2018. Montmorillonite dissolution kinetics: Experimental and reactive transport modeling interpretation. Geochimica et Cosmochimica Acta, 227: 96-122.

Carroll, S.A., Walther, J.V., 1990. Kaolinite dissolution at 25°, 60°, and 80° C. American Journal of Science, 290(7): 797-810.

Chin, P.-K.F., Mills, G.L., 1991. Kinetics and mechanisms of kaolinite dissolution: effects of organic ligands. Chemical Geology, 90(3): 307-317.

Devidal, J.-L., Schott, J., Dandurand, J.-L., 1997. An experimental study of kaolinite dissolution and precipitation kinetics as a function of chemical affinity and solution composition at 150°C, 40 bars, and pH 2, 6.8, and 7.8. Geochimica et Cosmochimica Acta, 61(24): 5165-5186.

Dove, P.M., Platt, F.M., 1996. Compatible real-time rates of mineral dissolution by Atomic Force Microscopy (AFM). Chemical Geology, 127(4): 331-338.

Drever, J.I., Stillings, L.L., 1997. The role of organic acids in mineral weathering. Colloids and Surfaces A: Physicochemical and Engineering Aspects, 120(1): 167-181.

Fischer, C., Arvidson, R.S., Lüttge, A., 2012. How predictable are dissolution rates of crystalline material? Geochimica et Cosmochimica Acta, 98(0): 177-185.

Furrer, G., Stumm, W., 1986. The coordination chemistry of weathering: I. Dissolution kinetics of δ-Al2O3 and BeO. Geochimica et Cosmochimica Acta, 50(9): 1847-1860.

Furrer G., Zysset M., and Schindler P. W. (1993) Weathering kinetics of montmorillonite: Investigations in batch and mixed-flow reactors. In Geochemistry of Clay-Pore Fluid Interactions (ed. D. A. C. Manning, P. L. Hall, and C. R. Hughes) Vol. 13, pp. 243–262. Chapman & Hall.

Ganor, J., Mogollón, J.L., Lasaga, A.C., 1995. The effect of pH on kaolinite dissolution rates and on activation energy. Geochimica et Cosmochimica Acta, 59(6): 1037-1052.

Ganor, J., Reznik, I.J., Rosenberg, Y.O., 2009. Organics in Water-Rock Interactions. Reviews in Mineralogy and Geochemistry, 70(1): 259-369.

Gilkes, R., Young, R., Quirk, J., 1972. The oxidation of octahedral iron in biotite.

Golubev, S.V., Bauer, A., Pokrovsky, O.S., 2006. Effect of pH and organic ligands on the kinetics of smectite dissolution at 25°C. Geochimica et Cosmochimica Acta, 70(17): 4436-4451.

Grasshoff, K., Kremling, K., Ehrhardt, M., 2009. Methods of seawater analysis. John Wiley & Sons.

Haward, S.J. et al., 2011. In situ atomic force microscopy measurements of biotite basal plane reactivity in the presence of oxalic acid. Geochimica et Cosmochimica Acta, 75(22): 6870-6881.

Hodson, M.E., 2006. Does reactive surface area depend on grain size? Results from pH 3, 25 °C far-from-equilibrium flow-through dissolution experiments on anorthite and biotite. Geochimica et Cosmochimica Acta, 70(7): 1655-1667.

Howard, A.G., Coxhead, A.J., Potter, I.A., Watt, A.P., 1986. Determination of dissolved aluminium by the micelle-enhanced fluorescence of its lumogallion complex. Analyst, 111(12): 1379-1382.

Huertas, F.J., Chou, L., Wollast, R., 1999. Mechanism of kaolinite dissolution at room temperature and pressure Part II: kinetic study. Geochimica et Cosmochimica Acta, 63(19-20): 3261-3275.

Hughes, C.R. et al., 1990. Selected Applications of Analytical Electron Microscopy in Clay Mineralogy. In: Mackinnon, I.D.R., Mumpton, F.A. (Eds.), Electron–Optical Methods in Clay Science. Clay Minerals Society, pp. 0.

Kalinowski, B.E., Schweda, P., 1996. Kinetics of muscovite, phlogopite, and biotite dissolution and alteration at pH 1-4, room temperature. Geochimica et Cosmochimica Acta, 60(3): 367-385.

Kalinowski, B.E., Schweda, P., 2007. Rates and nonstoichiometry of vermiculite dissolution at 22°C. Geoderma, 142(1): 197-209.

Köhler, S.J., Dufaud, F., Oelkers, E.H., 2003. An experimental study of illite dissolution kinetics as a function of ph from 1.4 to 12.4 and temperature from 5 to 50°C. Geochimica et Cosmochimica Acta, 67(19): 3583-3594.

Kurganskaya, I., Arvidson, R.S., Fischer, C., Luttge, A., 2012. Does the stepwave model predict mica dissolution kinetics? Geochimica et Cosmochimica Acta, 97(0): 120-130.

Kurganskaya, I., Luttge, A., 2013. A comprehensive stochastic model of phyllosilicate dissolution: Structure and kinematics of etch pits formed on muscovite basal face. Geochimica et Cosmochimica Acta, 120(0): 545-560.

Kuwahara, Y., 2008. In situ observations of muscovite dissolution under alkaline conditions at 25-50°C by AFM with an air/fluid heater system. American Mineralogist, 93(7): 1028-1033.

Lamarca-Irisarri D., Van Driessche E.S., Jordan G., Cappelli C., Huertas F.J., 2019. The role of pH, temperature, and $NH4^+$ during mica weathering. ACS Earth Space Chem. 2019, 3, 11, 2613–2622.

Lammers, K., Smith, M.M., Carroll, S.A., 2017. Muscovite dissolution kinetics as a function of pH at elevated temperature. Chemical Geology, 466: 149-158.

Lasaga, A.C., 1998. Kinetic Theory in the Earth Sciences. Princeton Series in Geochemistry. Princeton University Press, New Jersey.

Lasaga, A.C., Luttge, A., 2001. Variation of Crystal Dissolution Rate Based on a Dissolution Stepwave Model. Science, 291(5512): 2400-2404.

Lazic, D. et al., 2010. Stability of tris-1, 10-phenanthroline iron (II) complex in different composites. Chemical Industry andChemical Engineering Quarterly, 16(2): 193-198.

Li, J., Zhang, W., Li, S., Li, X., Lu, J., 2014. Effects of citrate on the dissolution and transformation of biotite, analyzed by chemical and atomic force microscopy. Applied Geochemistry, 51: 101-108.

Lüttge, A., Arvidson, R.S., Fischer, C., 2013. Fundamental Controls of Dissolution Rate Spectra: Comparisons of Model and Experimental Results. Procedia Earth and Planetary Science, 7: 537-540.

Luttge, A., Arvidson, R.S., Fischer, C., Kurganskaya, I., 2019. Kinetic concepts for quantitative prediction of fluid-solid interactions. Chemical Geology, 504: 216-235.

Malmström, M., Banwart, S., 1997. Biotite dissolution at 25°C: The pH dependence of dissolution rate and stoichiometry. Geochimica et Cosmochimica Acta, 61(14): 2779-2799.

Malmström, M., Banwart, S., Lewenhagen, J., Duro, L., Bruno, J., 1996. The dissolution of biotite and chlorite at 25°C in the near-neutral pH region. Journal of Contaminant Hydrology, 21(1-4): 201-213.

McMaster, T.J. et al., 2008. High-resolution imaging of biotite dissolution and measurement of activation energy. Mineralogical Magazine, 72(1): 115-120.

Metz, V., Amram, K., Ganor, J., 2005. Stoichiometry of smectite dissolution reaction. Geochimica et Cosmochimica Acta, 69(7): 1755-1772.

Murakami, T., Utsunomiya, S., Yokoyama, T., Kasama, T., 2003. Biotite dissolution processes and mechanisms in the laboratory and in nature: Early stage weathering environment and vermiculitization. American Mineralogist, 88(2-3): 377-386.

Nagy, K.L., Blum, A.E., Lasaga, A.C., 1991. Dissolution and precipitation kinetics of kaolinite at 80 degrees C and pH 3; the dependence on solution saturation state. Am J Sci, 291(7): 649-686.

Oelkers, E.H., Schott, J., Gauthier, J.-M., Herrero-Roncal, T., 2008. An experimental study of the dissolution mechanism and rates of muscovite. Geochimica et Cosmochimica Acta, 72(20): 4948-4961.

Pachana, K., Zuddas, P., Censi, P., 2012. Influence of pH and temperature on the early stage of mica alteration. Applied Geochemistry, 27(9): 1738-1744.

Peacor, D.R. (1992) Analytical electron microscopy: X-ray microanalysis. Pp. 335380 in: Minerals and Reactions at the Atomic Scale: Transmission Electron Microscopy (P.R. Buseck, editor). Reviews in Mineralogy, 27. Mineralogical Society of America, Washington, D.C.

Pyenson, H., Tracy, P.H., 1945. A 1,10—Phenanthroline Method for the Determination of Iron in Powdered Milk. Journal of dairy science, 28(5): 401-412.

Ramos, M.E., Cappelli, C., Rozalén, M., Fiore, S., Huertas, F.J., 2011. Effect of lactate, glycine, and citrate on the kinetics of montmorillonite dissolution. American Mineralogist, 96(5-6): 768-780.

Ramos, M.E., Garcia-Palma, S., Rozalen, M., Johnston, C.T., Huertas, F.J., 2014. Kinetics of montmorillonite dissolution: An experimental study of the effect of oxalate. Chemical Geology, 363(0): 283-292.

Rozalen, M., Huertas, F.J., 2013. Comparative effect of chrysotile leaching in nitric, sulfuric and oxalic acids at room temperature. Chemical Geology, 352(0): 134-142.

Rozalén, M.L. et al., 2008. Experimental study of the effect of pH on the kinetics of montmorillonite dissolution at 25°C. Geochimica et Cosmochimica Acta, 72(17): 4224-4253.

Rufe, E., Hochella, M.F., 1999. Quantitative assessment of reactive surface area of phlogopite during acid dissolution. Science, 285(5429): 874-876.

Samson, S.D., Nagy, K.L., Cotton Iii, W.B., 2005. Transient and quasi-steady-state dissolution of biotite at 22-25°C in high pH, sodium, nitrate, and aluminate solutions. Geochimica et Cosmochimica Acta, 69(2): 399-413.

Satoh, H., Ishii, T., Owada, H., 2013. Dissolution of compacted montmorillonite at hyperalkaline pH and 70°C: in situ VSI and ex situ AFM measurements. Clay Minerals, 48(2): 285-294.

Smith, M.M., Dai, Z., Carroll, S.A., 2017. Illite dissolution kinetics from 100 to 280°C and pH 3 to 9. Geochimica et Cosmochimica Acta, 209: 9-23.

Swoboda-Colberg, N.G., Drever, J.I., 1993. Mineral dissolution rates in plot-scale field and laboratory experiments. Chemical Geology, 105(1–3): 51-69.

Taylor, A.S., Blum, J.D., Lasaga, A.C., MacInnis, I.N., 2000. Kinetics of dissolution and Sr release during biotite and phlogopite weathering. Geochimica et Cosmochimica Acta, 64(7): 1191-1208.

Turpault, M.P., Trotignon, L., 1994. The dissolution of biotite single crystals in dilute HNO3 at 24°C: Evidence of an anisotropic corrosion process of micas in acidic solutions. Geochimica et Cosmochimica Acta, 58(13): 2761-2775.

Ullman, W.J., Welch, S.A., 2002. Organic Ligands and Feldspar Dissolution. In: Hellmann, R., Wood, S.A. (Eds.), Water-Rock Interactions, Ore Deposits, and Environmental Geochemistry. A tribute to David A. Crerar. Geochemical Society Special Publication, pp. 3-35.

Van Driessche, A.E.S., Sleutel, M., 2013. In situ measurement of crystal surface dynamics in pure and contaminated solutions by Confocal Microscopy and Atomic Force Microscopy. Crystal Research and Technology, 48(10): 919-941.

Voinot, A. et al., 2013. Experimental dissolution vs. transformation of micas under acidic soil conditions: Clues from boron isotopes. Geochimica et Cosmochimica Acta, 117(0): 144-160.

Welch, S.A., Ullman, W.J., 1996. Feldspar dissolution in acidic and organic solutions: Compositional and pH dependence of dissolution rate. Geochimica et Cosmochimica Acta, 60(16): 2939-2948.

Wieland, E., Stumm, W., 1992. Dissolution kinetics of kaolinite in acidic aqueous solutions at 25°C. Geochimica et Cosmochimica Acta, 56(9): 3339-3355.

Wolery, T.J., 1992. EQ3NR, A Computer Program for Geochemical Aqueous Speciation-Solubility Calculations: Theoretical Manual, User's Guide, and Related Documentation (Version 7.0).

Xue, X., Wang, W., Fan, H., Xu, Z., Pedruzzi, I., Li, P., Yu, J., 2019. Adsorption behavior of oxalic acid at water–feldspar interface: experiments and molecular simulation. Adsorption 25, 1191-1204.

Yang, L., Steefel, C.I., 2008. Kaolinite dissolution and precipitation kinetics at 22 °C and pH 4. Geochimica et Cosmochimica Acta, 72(1): 99-116.

Yokoyama, S., Kuroda, M., Sato, T., 2005. Atomic force microscopy study of montmorillonite dissolution under highly alkaline conditions. Clays and Clay Minerals, 53(2): 147-154.

Zhang, L., Jun, Y.-S., 2015. Distinctive Reactivities at Biotite Edge and Basal Planes in the Presence of Organic Ligands: Implications for Organic-Rich Geologic CO_2 Sequestration. Environmental Science and Technology, 49(16), 10217–10225.

Zysset, M., Schindler, P.W., 1996. The proton promoted dissolution kinetics of K-montmorillonite. Geochimica et Cosmochimica Acta, 60(6): 921-931.

Declaration of interests

☒ The authors declare that they have no known competing financial interests or personal relationships that could have appeared to influence the work reported in this paper.

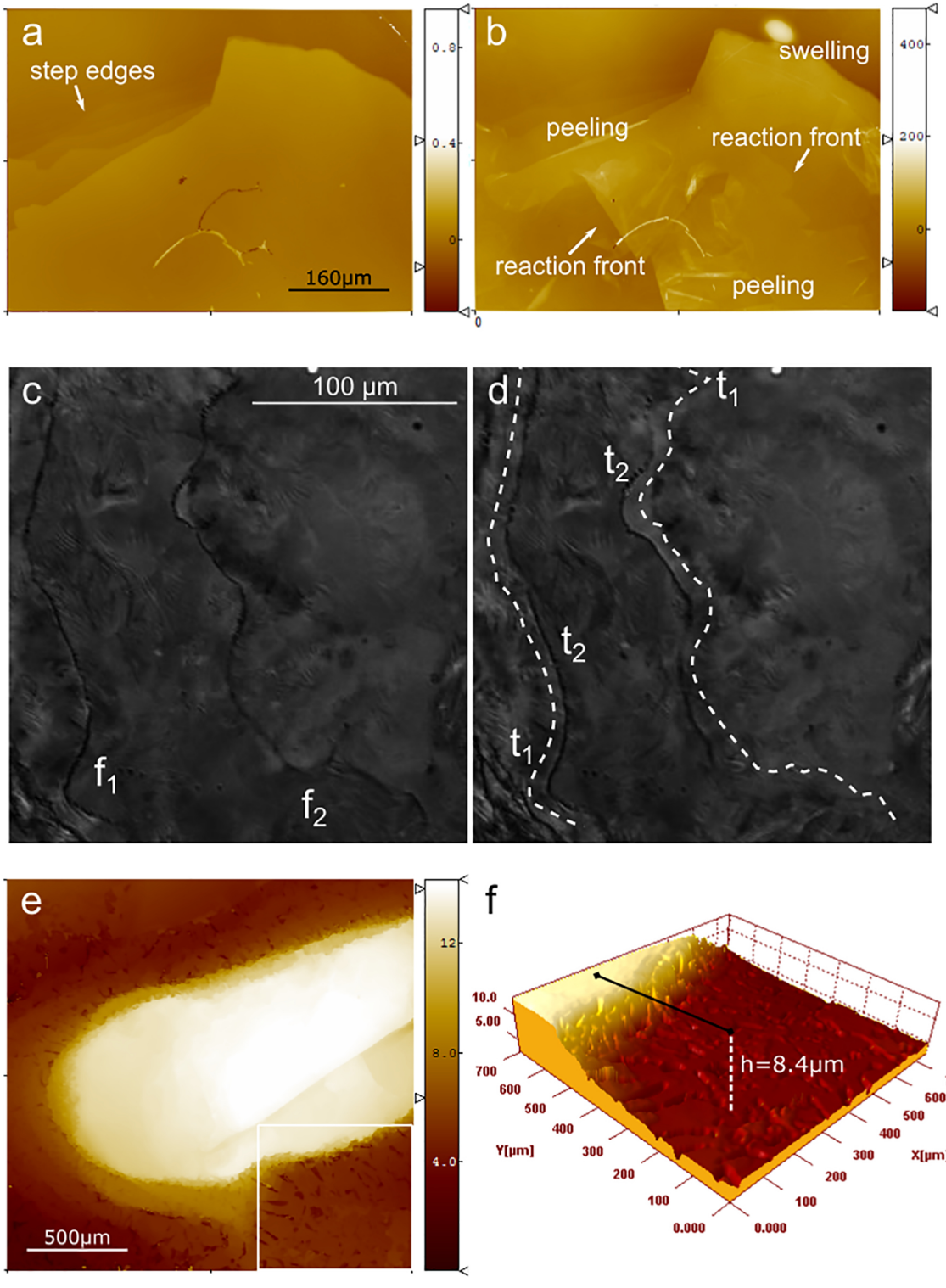
a
step edges
160µm
0.8
0.4
0
b
swelling
peeling
reaction front
reaction front
peeling
400
200
0
c
100 µm
f1
f2
d
t1
t2
t2
t1
e
500µm
12
8.0
4.0
f
h=8.4µm
10.0
5.00
Y[µm]
X[µm]
700
600
500
400
300
200
100
0.000

Figure 1

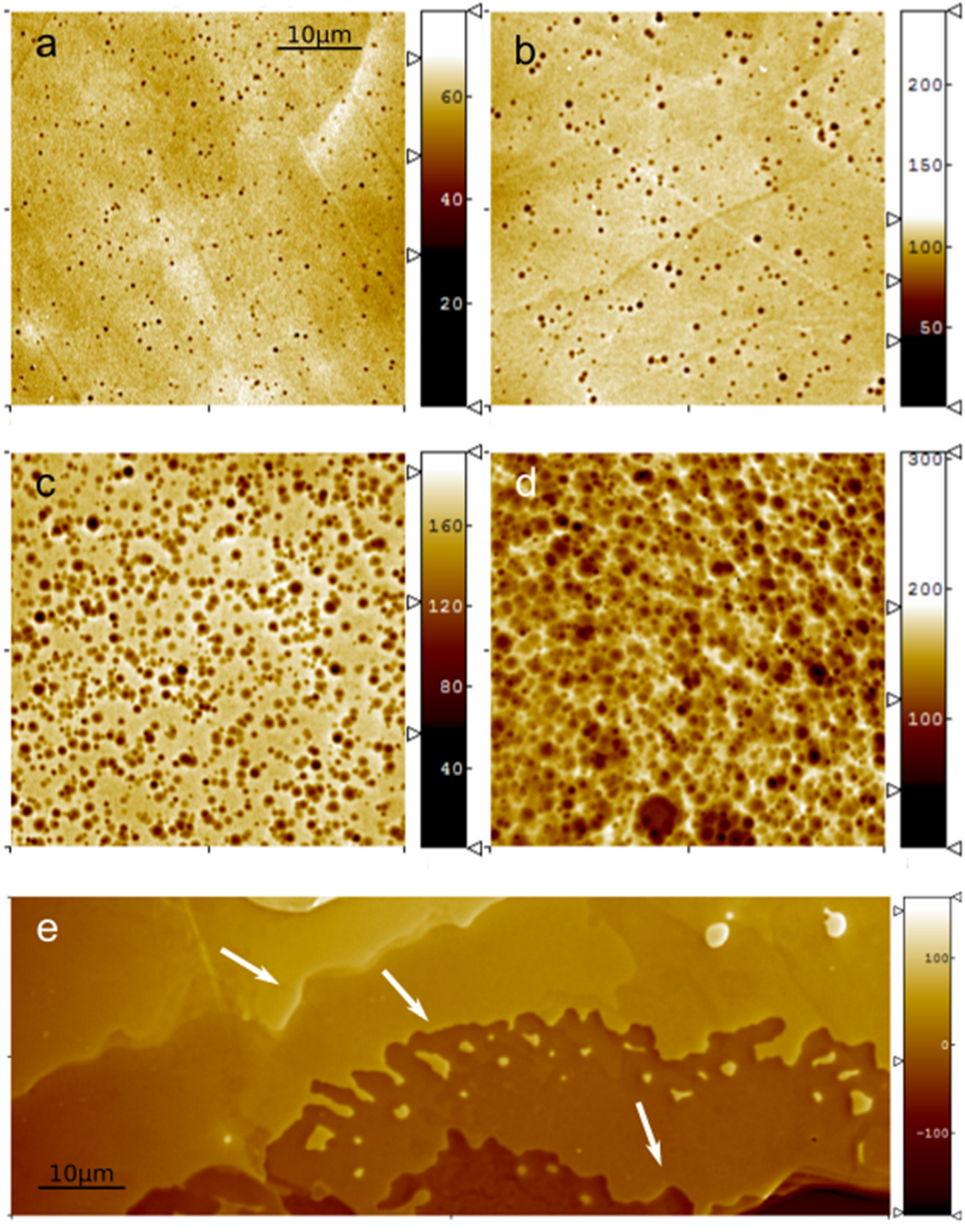
a
10µm
60
40
20
b
200
150
100
50
c
160
120
80
40
d
300
200
100
e
100
0
-100
10µm

Figure 2

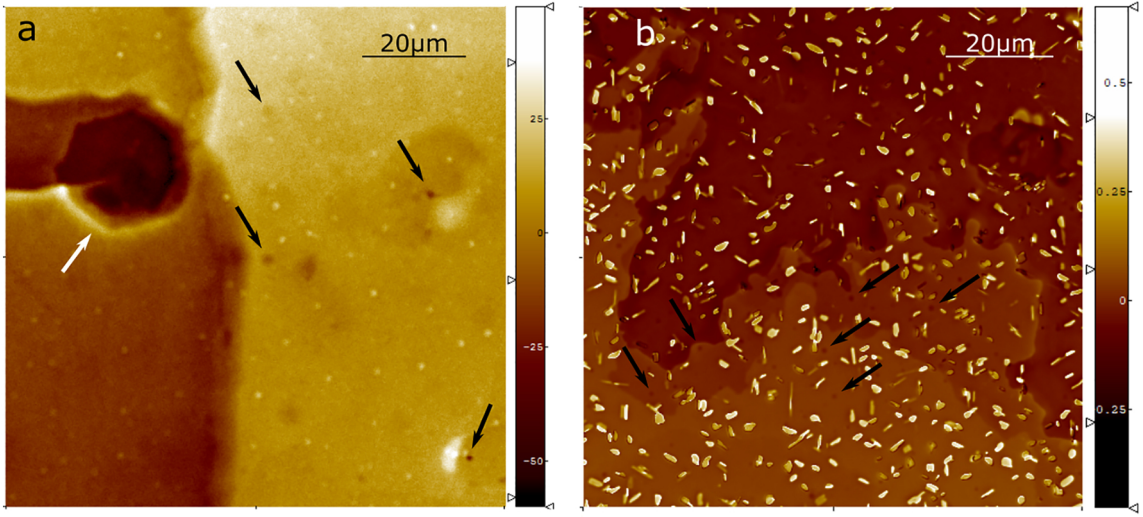

Figure 3

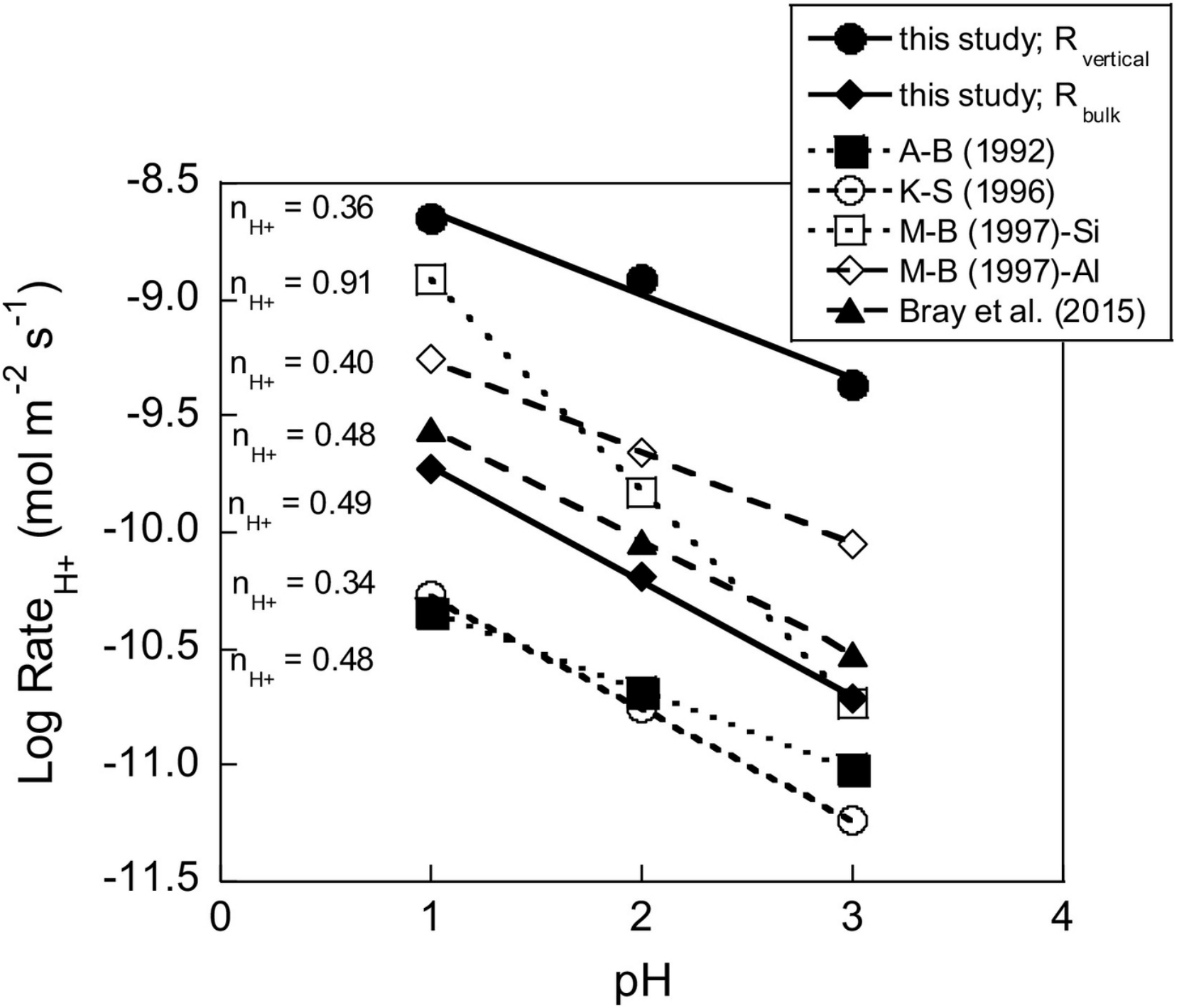
this study; R vertical
this study; R bulk
A-B (1992)
K-S (1996)
M-B (1997)-Si
M-B (1997)-Al
Bray et al. (2015)
n H+ = 0.36
n H+ = 0.91
n H+ = 0.40
n H+ = 0.48
n H+ = 0.49
n H+ = 0.34
n H+ = 0.48
Log Rate H+ (mol m-2 s-1)
-8.5
-9.0
-9.5
-10.0
-10.5
-11.0
-11.5
0
1
2
3
4
pH

Figure 4

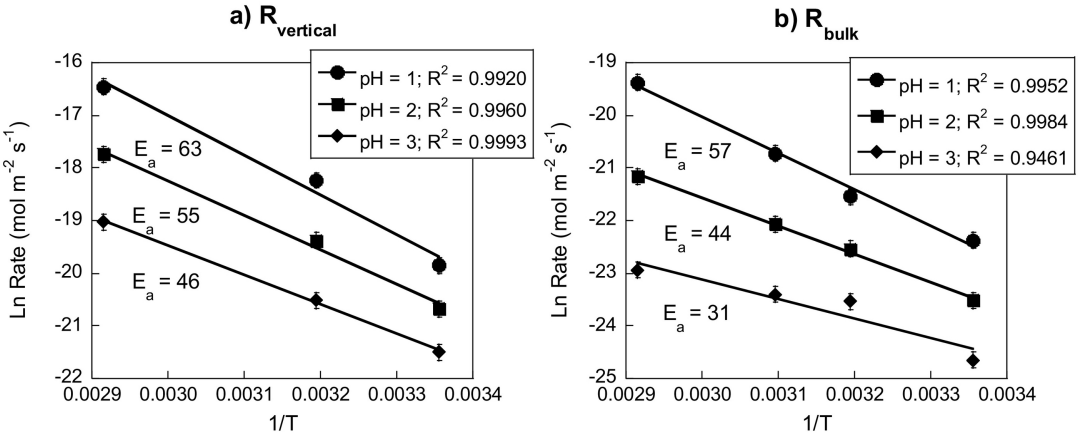
a) R vertical
pH = 1; R2 = 0.9920
pH = 2; R2 = 0.9960
pH = 3; R2 = 0.9993
Ea = 63
Ea = 55
Ea = 46
Ln Rate (mol m-2 s-1)
1/T
b) R bulk
pH = 1; R2 = 0.9952
pH = 2; R2 = 0.9984
pH = 3; R2 = 0.9461
Ea = 57
Ea = 44
Ea = 31
Ln Rate (mol m-2 s-1)
1/T

Figure 5